A new multi-grid bathymetric dataset of the Gulf of Naples (Italy) from complementary multi-beam echosounders

Federica Foglini[1], Marzia Rovere[1], Renato Tonielli[1], Giorgio Castellan[1,2*], Mariacristina Prampolini[1,2], Francesca Budillon[1], Marco Cuffaro3, Gabriella Di Martino[1], Valentina Grande[1], Sara Innangi[1], Maria Filomena Loreto[1], Leonardo Langone[4], Fantina Madricardo[1], Alessandra Mercorella[1], Paolo Montagna4, Camilla Palmiotto[1], Claudio Pellegrini[1], Antonio Petrizzo[1], Lorenzo Petracchini[3], Alessandro Remia[1], Marco Sacchi[1], Daphnie Sanchez Galvez[1], Anna Nora Tassetti[5], Fabio Trincardi[6].

[1] CNR –ISMAR - National Research Council, Institute of Marine Sciences, Italy;
2 NBFC - National Biodiversity Future Centre, Italy
[3] CNR-IGAG - National Research Council, Institute of Environmental Geology and Geoengineering, Italy;
[4] CNR ISP - National Research Council, Institute of Polar Sciences, Italy;
[5] CNR IRBIM- National Research Council, Institute for Biological Resources and Marine Biotechnologies, Italy;
[6] CNR-DSSTTA - National Research Council, Department of Earth Systems Science and Environmental Technologies, Italy.

Correspondence to: giorgio.castellan@cnr.it

Abstract

High-resolution bathymetry provides critical information to marine geoscientists. Bathymetric big data help characterise the seafloor and its benthic habitats, understand sedimentary records, and support the development of offshore engineering infrastructures. From September 27th to October 20th, 2022, the new CNR Research Vessel Gaia Blu explored the seafloor of the Naples and Pozzuoli Gulfs, and the Amalfi coastal area (Tyrrhenian Sea, Italy) from 50 to more than 2000 m water depth, acquiring about 5000 km^2 of multi beam echosounder data. This area is particularly vulnerable to abrupt changes driven by the dynamics of several volcanic complexes, active in the area, and by human-induced impacts reflecting the proximity to the highly populated and touristic coastal area of Naples and nearby famous islands. For these reasons, the seafloor of the area needs to be known and constantly monitored. The digital bathymetric data previously available are restricted to the shallow highly dynamic area of the Gulf of Naples and appear fragmented as they were acquired in successive years, with different goals thereby using a variety of devices, with markedly different spatial resolutions. In this paper, we present bathymetric maps of the Gulf of Naples and adjacent slope basins at unprecedented resolution using three state-of-the-art multi beam echosounders. These high-resolution data highlight the technological advances of geophysical surveys achieved over the last 20 years and contribute to assessing the most dynamic areas where changes in the seafloor over time can be quantified. The new digital multi-resolution bathymetric products are openly accessible via Marine Geosciences Data System MGDS (refer to

section Data Availability, Table 8, for datasets and products DOIs), perfectly matching the FAIR (Findable, Accessible, Interoperable and Reusable) and Open Science Principles.

1. Introduction

In 2018, GEBCO and the Nippon Foundation joined forces to establish the Nippon Foundation GEBCO Seabed 2030 Project (Mayer et al., 2018), an international effort to foster the complete mapping of the world ocean by 2030. Despite many years of mapping efforts unveiled increasingly larger portions of the seabed, only about 25% of the world oceans seafloor is mapped to date at high resolution (https://seabed2030.org/our-mission/). Obtaining a high-resolution map of the world's seafloor is crucial to understanding how oceans work, from geodynamics and geohazards aspects, to the interactions between seafloor morphology and bottom-current dynamics, and to the distribution and ecological status of benthic habitats to cite a few applications. In the last 40 years, almost two-thirds of marine environments have been "severely altered" by human activity (Díaz et al., 2019) resulting in significant biodiversity loss and erosion of the ecological services and goods (Worm et al., 2006). In this context, the European Union has implemented a governance framework specifically aiming at assessing, monitoring, and preserving the status of the marine benthic natural heritage (Marine Strategy Framework Directive MSFD, 2014/89/EU), but also at promoting the sustainable exploitation of marine and coastal resources (European MSP Directive, 2008/56/EC). Among the European Seas, the Mediterranean Sea is a hotspot of biodiversity, hosting more than 7.5% of global biodiversity (Bianchi and Morri, 2000) with a high percentage of endemic species (Myers et al., 2000) and unique ecosystems. However, the basin is recognized to be "under siege" due to the historical and still ongoing impacts from multiple stressors such as littering and dumping, trawling, ghost fishing, seaborne traffic and modification of the seafloor (Coll et al., 2012; Puig et al., 2012; Madricardo et al., 2017, 2019; Canals et al., 2021; Budillon et al., 2022; Pellegrini et al., 2023; Trincardi et al., 2023). This is particularly evident in the Gulf of Naples, a densely populated coastal region stretching along 385 km on the eastern Tyrrhenian Sea, which represents an important tourist destination including the Gulf Islands (Capri, Ischia and Procida), Sorrento Peninsula, Vesuvius National Park, Phlegraean Fields and archaeological sites of Pompeii, Herculaneum, Pozzuoli and Cuma.

The underwater landscape of the Gulf of Naples is geomorphologically complex, with large canyon systems, marine landslides, debris flow deposits, volcanic apparatuses; the area includes various benthic habitats of ecological relevance from the shore to the deep sea, such as *Posidonia oceanica* meadows (e.g., MATTM, 2004), animal forests (e.g., Bavestrello et al., 2014), cold-water corals (CWC, Taviani et al., 2019; Angiolillo et al., 2023), and hydrothermal vent communities (e.g. Apolloni et al., 2020; Donnarumma et al., 2019). The gulf region also hosts numerous archaeological and cultural heritage sites, threatened by natural and human pressures (Mattei et al. 2019). To preserve marine biodiversity and the historical value of the area, four Marine Protected Areas (MPAs) have been established: the Underwater Parks of Baia and Gaiola MPAs, the Regno di Nettuno MPA and the Punta Campanella MPA (Apolloni et al., 2018).

The first extensive high-resolution mapping of the seafloor of the gulf was performed in the framework of the Italian geological mapping research program (1997-2017) through bathymetric surveys of the continental shelf/slope system of the Campania region, using numerous multi beam echosounder systems (MBESs) with avertical resolution of < 0.25% of the water depth and position accuracy better than 10 m. The data, acquired at different resolutions, were merged to create a Digital Terrain Model (DTM) with a homogeneous grid and with a cell spacing of 20 m (Aiello et al., 2020). This map highlighted the most prominent geomorphological features in the coastal zone such as the canyons, banks, debris avalanches, hydrothermal vents and volcanoclastic basement outcrops with high ecological value habitats in urgent need of preservation (Taviani et al 2019). This valuable dataset was shared in gridded form, within the EMODnet project, as 1/16 arc minutes (ca. 115 m) DTMs. High-resolution data for selected areas are also available as 1/128 or 1/256 arc minutes (ca.15 m or 7 m) HR-DTMs (https://emodnet.ec.europa.eu/geoviewer/).

Despite the significant effort of ongoing national and international projects and infrastructures worldwide to make data available, such as GEBCO (https://www.gebco.net) and EMODnet (https://emodnet.ec.europa.eu/en), local high-resolution datasets and raw data are typically not yet accessible (Sievers et al., 2021). Indeed, local datasets are often generated, hosted, and administered by various institutes in the world with dissimilar data policies, which often do not follow the Findable, Accessible, Interoperable and Reusable (FAIR) data principles (Stall et al., 2019).

This study presents the results of a high-resolution geophysical survey named JammeGaia22 conducted in October 2022 on board R/V Gaia Blu using three different state-of-the-art MBESs (Kongsberg EM 2040, EM 712, and EM 304) and aims at improving the knowledge of the seascape of the Gulf of Naples by enhancing the analysis/visualization of seabed morphology through high-resolution digital bathymetric models.

Our contribution aims at highlighting the innovative approach used during JammeGaia22 (Section Multibeam data processing), where data are processed daily on board and can be made available to the scientific community and the generic public in very short time via a geoportal, making the datasets FAIR and facilitating interdisciplinary research within the Open Science Principles. We describe the bathymetric and backscatter datasets in detail highlighting its potential applications (Section Results and discussion) thanks to the good quality of the data collection discussed in the section Data Quality. Finally, we provide full access to the whole dataset, the bathymetric grids and backscatter mosaics produced, and the metadata as explicated in section Data availability.

Given the unprecedented high- and multi-resolution survey conducted in the study area and the availability of ancillary data such as backscatter and water-column data, this dataset represents a unique benchmark for future studies related to geohazards assessment, sediment transport, fishery management, resource exploration and sustainable exploitation, maritime spatial planning and decision making, marine ecosystem and habitat mapping, oceanographic modeling including storm surges and scenarios of tsunami wave propagation.

2 Study area - Geological and geomorphological background

The investigated area belongs to the central-eastern margin of the Tyrrhenian Sea, encompassing the region between the western margin of the Southern Apennines thrust belt and the Tyrrhenian abyssal plain (ca.3000 m deep; Figure 1). The Tyrrhenian Sea is the youngest back-arc basin of the Mediterranean Sea that developed since the Middle Miocene (Trincardi and Zitellini, 1987; Kastens et al., 1988; Lymer et al., 2018; Loreto et al., 2021; Miramontes et al., 2023) reflecting the east- and south-eastward retreat of the Ionian slab, guided by the Africa-Europe convergence (Moussat et al., 1985; Malinverno and Ryan, 1986; Kastens et al., 1988). The Campania segment of the eastern Tyrrhenian margin is characterized by a series of NE-SW trending half-graben bounded by structural highs that have developed since the early Pleistocene and accommodate the tectonic-controlled subsidence of the alluvial plains along with their submerged counterparts, namely the Gaeta Gulf, the Gulf of Naples and the Gulf of Salerno (Figure 1; Romano et al., 1984; Ruberti et al., 2022; Amato et al., 2011; Bellucci et al., 2006).

Structural lineaments also control the preferential pathways of volcanic activity, particularly in the last 2 My. Volcanic activity followed an eastward migration, governing the geomorphological setting of the region and promoting deposition of sedimentary sequences up to 3 km thick (Milia, 1999; Milia et al., 2003).The Phlegraean Fields volcanic area is a 78-ka old active poly-calderic system (Scarpati et al., 2012) that has affected its territory in the last millennia and has strongly influenced the evolution of the adjacent coasts during the late Pleistocene and Holocene, which has been mainly shaped by three super-eruptions. The oldest one was the Campanian Ignimbrite (CI) eruption that occurred at ca. 35-40 ka BP (Giaccio et al., 2017). After this main event, the northern part of the just-formed caldera was submerged by the sea. The second eruption, which led to the formation of the Masseria Del Monte Tuff, occurred at 29.3 ka BP (Albert et al., 2019). The Neapolitan Yellow Tuff (NYT; Deino et al. 2004) eruption at ca. 15 ka BP contributed to the formation of the youngest caldera (Orsi et al., 1992), nowadays well documented also offshore (Sacchi et al., 2014; Steinmann et al., 2016, 2018). Besides volcanic eruptions, alternating long-term magma/hydrothermal fluid inflation and deflation processes controlled the morphological evolution of this area. Further, short-term vertical, meter-scale, ground movements characterised times immediately preceding and following each eruption, which produced rapid relative sea-level variations along the entire coastal sector (Isaia et al., 2019 and reference therein). The area has experienced high rates of subsidence (approx. 4.0 mm/yr) through the Pleistocene (Torrente et al., 2010; Milia et al., 2017; Iannace et al., 2018), accompanied by the activity of major NE–SW-striking faults. At present, intense seismicity, including the Md 4.0 earthquake occurred on 2nd October 2023, is instead associated to the 18.0 mm/yr uplift of the central portion of the Phlegraean Field area.

Volcanic activity, long-term vertical ground movements, glacio-eustasy and the rapid dismantling of the emerging landscapes have driven a rapid geomorphological evolution of the margin, resulting in steep slopes, canyoning, deep-sea fan accretion and gravitational slope instability. Extensive lateral collapses of the volcanic edifices have been documented offshore, south of

Ischia Island (Chiocci et al., 1998; Chiocci and de Alteriis, 2006; de Alteriis et al., 2010), possibly occurred also in historical time, and two others of minor extent to the west and north of Ischia Island (Budillon et al., 2003; Violante et al., 2003) and in the Gulf of Naples (Milia et al., 2008, 2012; Passaro et al., 2018). The rapid aggradation of volcaniclastic deposits in shallow marine environment and the entrance of pyroclastic flows into the seawater also led to seafloor instability and creep in the prodelta offshore the main rivers (Sacchi et al., 2005; 2009).

Three main turbiditic systems, namely Cuma, Magnaghi and Dohrn Canyons, and the deep structurally controlled Salerno Valley, have developed along with the rising of intra-slope reliefs and volcanic activity, and acted as main conduits delivering sediment towards deeper-water domains (Passaro et al., 2016). These features characterize the present-day seafloor morphology and, although partially inactive, are of paramount interest as hotspots of biodiversity in the Mediterranean Sea (e.g., Taviani et al., 2019; Mussi et al., 2022).

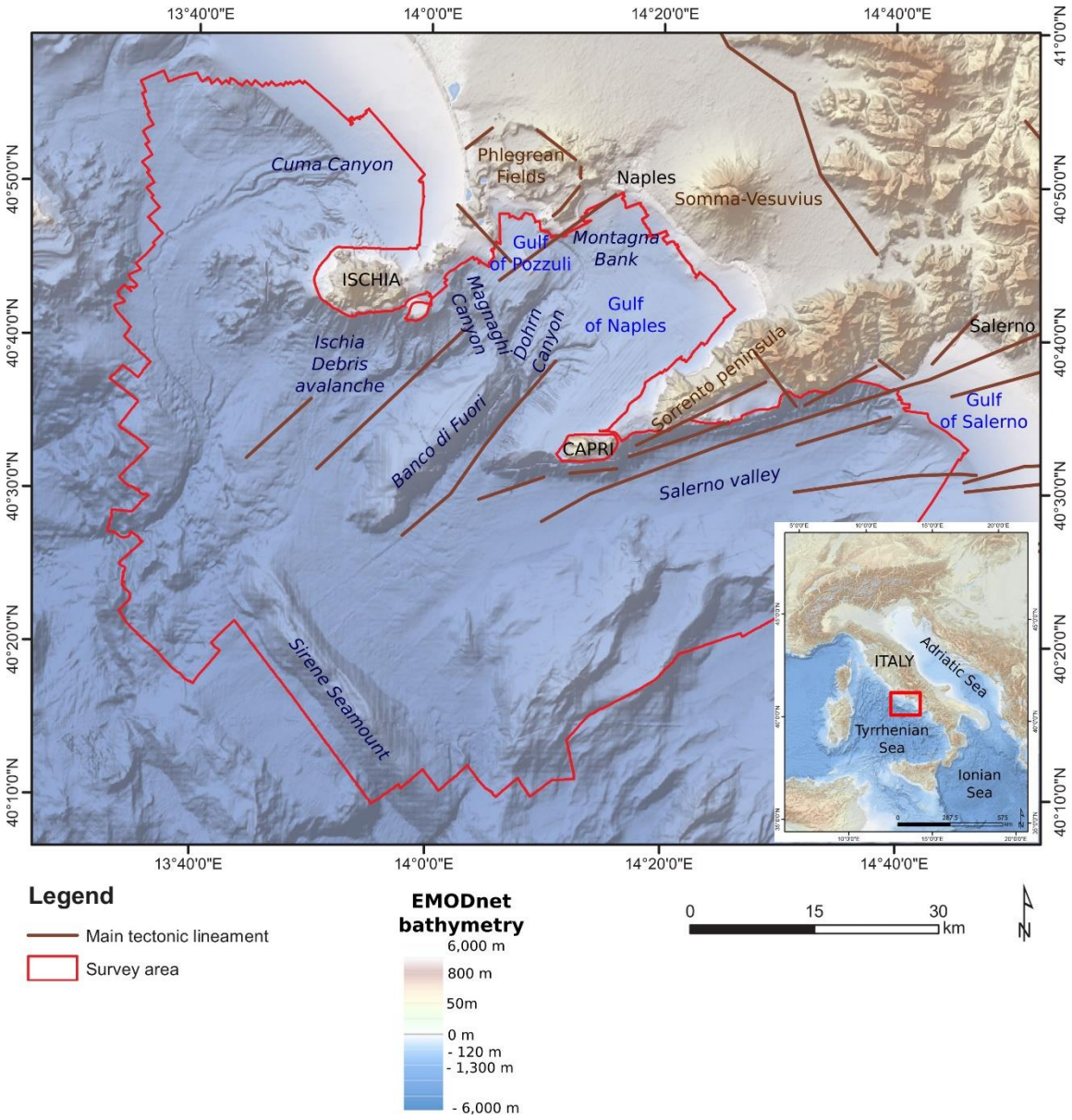

Figure 1. Map of the study area in the central Tyrrhenian Sea showing the main physiographic and tectonic features (modified from Aiello et al., 2020). Elevation and bathymetry from EMODnet bathymetry (https://emodnet.ec.europa.eu/en/bathymetry).

3. Materials and methods

3.1 Multi beam data acquisition

Multi beam data were collected during the JammeGaia22 cruise from September 27th to October 20th 2022 using three different MBES: the Kongsberg EM2040-04 MKII 0.4°x0.7° suited for water depths between 50 and 150 m, Kongsberg EM712 1°x0.5° for water depths between 150 and 1000 m and Kongsberg EM304 MKII 1°x1° for water depth greater than 1000 m (Table 1for acquisition settings).

Table 1. Acquisition settings for the three multi beam echosounder systems.

MBES	Water depth (m)	Frequency (kHz)	Angular coverage (degree)	Ping rate (Hz)	Acquisition mode
EM2040	50-100	300	65	1.5	Deep
EM2040	100-150	200	70	1.5	Very deep
EM712	150-600	70-100	70	2	Shallow
EM712	600-1000	40-100	70	2	Deep
EM304	>1000	30	65	>5	Auto

The MBESs were hull-mounted on the R/V Gaia Blu gondola with a T-configuration of linear transducer arrays. A Seapath 380 system was used for ship positioning, supplied by a Fugro HP differential Global Positioning System (DGPS), with Marinestar GNSS signal accuracy better than 5 cm. The Kongsberg motion sensor MRU (Motion Reference Unit) 5 and a Dual Antenna GPS integrated into the Seapath, were used to correct for pitch, roll, heave and yaw movements (reaching 0.02° roll and pitch accuracy, and 0.075° heading accuracy). A Valeport mini SVS sensor was positioned close to the transducers to measure the sound velocity for the beamforming. This sound velocity (SV) value was continuously compared to that from Sound velocity profiles (SVP) in use to warn when a new profile was required. However, the difference between SV from the SVS sensor and in-use profile never reached warning values since SVP were systematically collected at least twice a day with a Valeport Midas SVP, for a total of 40 SVPs. Data were logged, displayed and checked in real-time by the Kongsberg data acquisition and control software SIS 5 (Seafloor Information System). A tool included in SIS 5 software was used to extend the SVPs down to 12000 m water depth. Since the Mediterranean Sea is characterized by a stratified water column with peculiar changes in the physical-chemical properties (Tanhua et al. 2013; Rossi et al. 2014; Basterretxea et al. 2018), a linear regression based on the collected SVP data was run in R software (R Core Team, 2019) to estimate the sound velocity values down to 12000 m depth.

Professional topographers measured the offsets of the instruments with millimetric accuracy using a dedicated dimensional survey of the ship's hull at dry dock.

Sensors have been calibrated during the Sea Acceptance Tests (roll, pitch, time and heading offsets) and were also regularly checked in post-processing (Table 2 for calibration values).

Table 2. Calibration values applied after the Sea Acceptance Test.

MBES	Pitch	Roll	Heading
EM2040	+0.10°	+0.5°	-0.20°
EM304	00.00°	+0.2°	0.00°
EM712	-0.10°	-0.07°	-0.15°

We kept a 20% overlap between lines to ensure 100% of bathymetric coverage, avoiding the influence of external beams of bad quality given by possible residual errors in roll, sound speed profile measurements and poor seafloor detection. The multi beam operated with an average swath opening angle of about 65°/70° (Table 1) for each multi beam system. The vessel sailed with a reasonably constant speed of 8 knots, considered ideal to have the minimum noise and tested during the Sea Acceptance Test. Sea conditions were good and stable for the entire survey, with wave height almost always lower than 1 m. Seafloor and water column backscatter data were collected simultaneously during bathymetric data acquisition.

3.2 Multibeam data processing

The bathymetric data collected every day were processed on-board during nightshift to produce DTMs and backscatter mosaics, which were then uploaded the next morning in a dedicated WebGIS to inform the scientific community on the progress of the campaign and make the data openly available. The data processing workflow is summarized in Figure 2.

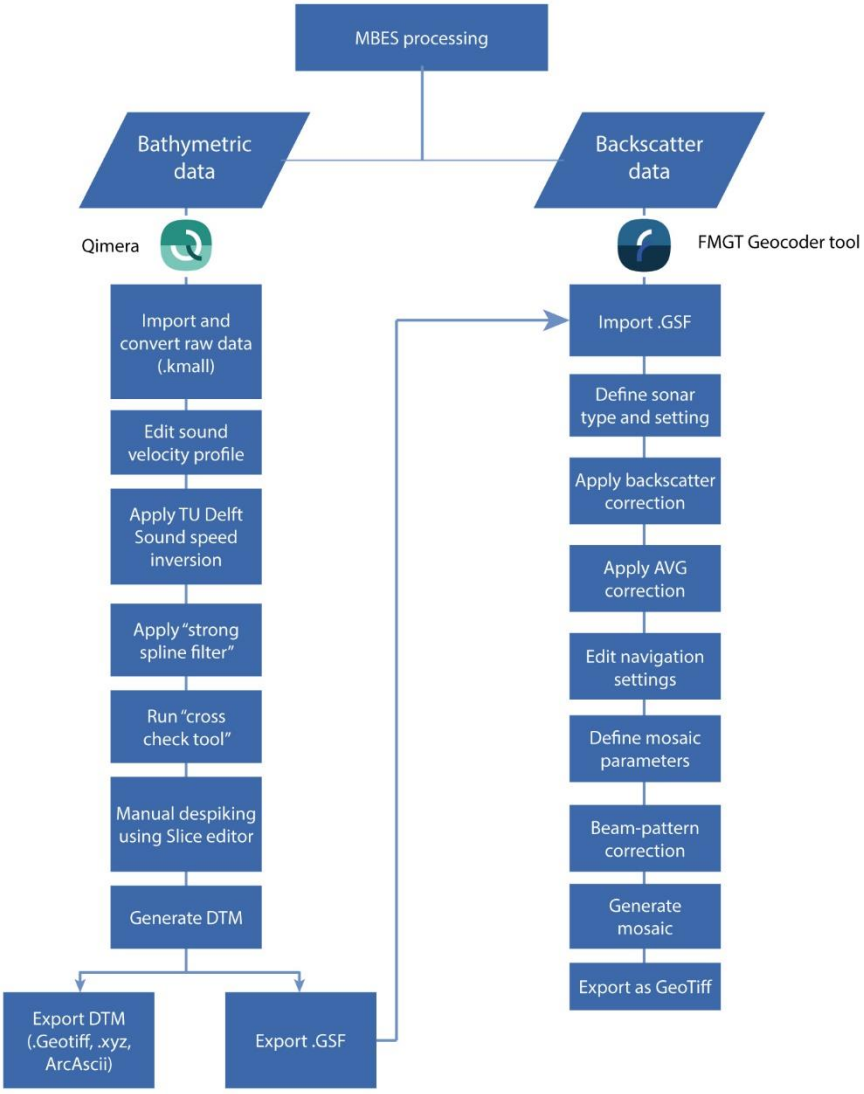

Figure 2. Workflow of bathymetric and backscatter data processing, described in 3.2.1 and 3.2.2

3.2.1 Bathymetric data processing

The processing of the raw data was carried out using the QPS Qimera v.2.5.0 software (Quality Positioning Services BV, Zeist, Netherlands) following a standard procedure, which includes sound speed correction, removal of erroneous soundings, and correction of vertical offsets from a previous swath. The quality of the data was initially checked using the 'Cross Check Tool' to check for soundings with significant offsets from the local mean water depth.

When sound velocity errors were evident in the data, the TU Delft Sound Speed Inversion tool (Beaudoin et al., 2018) was used to correct the profile. The tool applies an algorithm that allows a completely automated refraction error correction. It works by taking advantage of the overlap between survey lines to simultaneously estimate sound speed correction for a given set of pings and their neighbours, by computing a best-fit solution that minimizes the mismatch in the areas of overlap between lines (Mohammadloo et al., 2019). The settings applied for TU Delft Sound Inversion were data-specific, depending on the quality of the SVP, upon initial assessment.

After the sound speed correction, the strong spline filter of Qimera allowed removal of soundings beyond the local mean water depth (offsets); the remaining offsets (if any) were removed manually using the 'Slice editor' of Qimera. The processed bathymetric data were exported into GSF format for backscatter processing and to a gridded surface data (GeoTIFF). The resolution of the GeoTIFF was defined based on the water depth and the footprint calculated for each sonar used (Table 3).

Table 3. Calculated footprints of ensonified seafloor area at different water depths for each MBES, relative grid resolution chosen and mean of the number of soundings in each grid cell. Products and dataset are available at section Data Availability.

MBES	Water Depth (m)	TX Footprint (m)	RX Footprint (m)	Insonifed area (m^2)	Grid resolution (m)	Number of soundings per grid cell
EM2040 (0.4°x 0.7°)	50	0.4363	0.6109	0.92	2	7.12
	60	0.5236	0.7330	1.10		
	70	0.6109	0.8552	1.28		
	80	0.6981	0.9774	1.46		
	90	0.7854	1.0996	1.65		
	100	0.8727	1.2217	1.83		
EM712 (0.5°X1°)	150	1.3090	2.6181	3.28	5	23.87
	200	1.7453	3.4907	4.37		
	300	2.6180	5.2361	6.56	10	17.35
	400	3.4907	6.9815	8.75		
	500	4.3634	8.7269	10.94		
	600	5.2360	10.4722	13.12	15	9.96
	700	6.1087	12.2176	15.31		
	800	6.9814	13.9630	17.50	20	13.9
	900	7.8540	15.7084	19.69		
	1000	8.7267	17.4537	21.87		

EM304 (1°X1°)	1000	17.4537	17.4537	30.94	30	21.72
	1100	19.1991	19.1991	34.03		
	1200	20.9445	20.9445	37.12		
	1300	22.6899	22.6899	40.22	40	25.45
	1400	24.4352	24.4352	43.31		
	1500	26.1806	26.1806	46.40		
	1600	27.9260	27.9260	49.50		
	1700	29.6714	29.6714	52.59		
	1800	31.4167	31.4167	55.68		
	1900	33.1621	33.1621	58.78		
	2000	34.9075	34.9075	61.87		

3.2.2 Backscatter data post-processing

The MBES backscatter data were processed using the QPS Fledermaus Geocoder Tool (FMGT) v.7.10.2 software. The processed MBES data (.gsf) were used to apply backscatter corrections, beam pattern correction, and angle-varying gain (AVG) corrections to the backscatter data. After these corrections, FMGT applied the sonar's navigation data (i.e., XY coordinates, roll, heading, pitch, heave) to georeference the backscatter value. The DTM generated in Qimera provided a bathymetric grid to improve backscatter corrections. The reference grid was included by the FMGT software to determine topographic slope, while the corrected bathymetry in the source files (i.e., GSF) was regularly used to georeference the snippet trace from a single ping to the correct position on the seafloor (Quality Positioning Services B.V., 2020). Finally, the backscatter snippets were mosaicked with the 'No Nadir possible, 25% overlap' algorithm to reduce the banding effect, and 30-40% line blending was applied to blend the pixels in the overlapping areas. The mosaics were gridded in various resolutions (Table 4) with dB values cropped to ± 3σ and logarithmically mapped to 8-bit scale. These mosaics were exported as 'One merged Colored GeoTIFF format'.

Table 4. Resolution of backscatter mosaic for each MBES. Products and dataset are available at section Data Availability.

MBES	Mosaic resolution (m)
EM2040	5 m
EM712	10 m
EM304	30 m

3.3 Bathymetric derivatives

A geomorphometric analysis of the seabed was carried out using ArcGIS to emphasize any subtle variation in seafloor morphology. The geomorphometric indices calculated were slope, broad-scale and fine-scale Bathymetric Position Index (BPI), and vector ruggedness measure.

The slope is a first-order derivative of the bathymetry and represents seabed maximum inclination (in any direction) in degrees, the slope was measured in ArcGIS as the maximum rate of change in value from a cell to its immediate neighbours. The calculation is performed using the average maximum technique (Burrough and McDonell, 1998). picking an area of 3x3 pixels around each cell. Values are real numbers between 0.0° and 90.0°, areas of no data have a conventional value of -1.0. Depth values in input were smoothed before calculation of the slope using a user-defined smoothing window of 3x3. This approach served to removed local changes giving a regional value for slope and diminishing edge effect (Dolan, 2012).

Broad- and fine-scale BPIs were calculated using Benthic Terrain Modeler (BTM) toolbox for ArcGIS (Walbridge et al., 2018; Lundblad et al., 2006). BPI is derived from an input bathymetric data set and is a modification from topographic position index as defined by Weiss (2001) and Iampietro and Kvitek (2002). It evaluates differences in elevation between a focal point and the mean elevation of the surrounding cells within a user-defined window. Values range from -1 to +1, with negative values reflecting depressions in the seabed, null values for planar areas and positive values denoting positive reliefs. Broad-scale BPI allows the identification of main regional features within the seafloor, while fine-scale BPI helps identify smaller features of the benthic landscape. The values used to calculate BPIs for all the bathymetric surfaces are reported in Table 5.

Vector ruggedness measure (VRM) quantifies terrain ruggedness by measuring the dispersion of vectors orthogonal to the terrain surface (Sappington et al., 2007). VRM shows low values both in flat and steep areas, but high values in areas that are both steep and rugged.

4. Results and Discussion

4.1 Multi-grid bathymetric dataset

The bathymetric dataset covers an area of about 5000 km^2 offshore the Gulf of Naples from 50 to more than 2000 m water depth (Figure 3). The different resolutions, depending on the water depth and the MBES footprint, of the acquired data reveal

the complexity of the seafloor with unprecedented details and allow to better discriminate geomorphological features already described in the literature (D'Argenio et al., 2004).

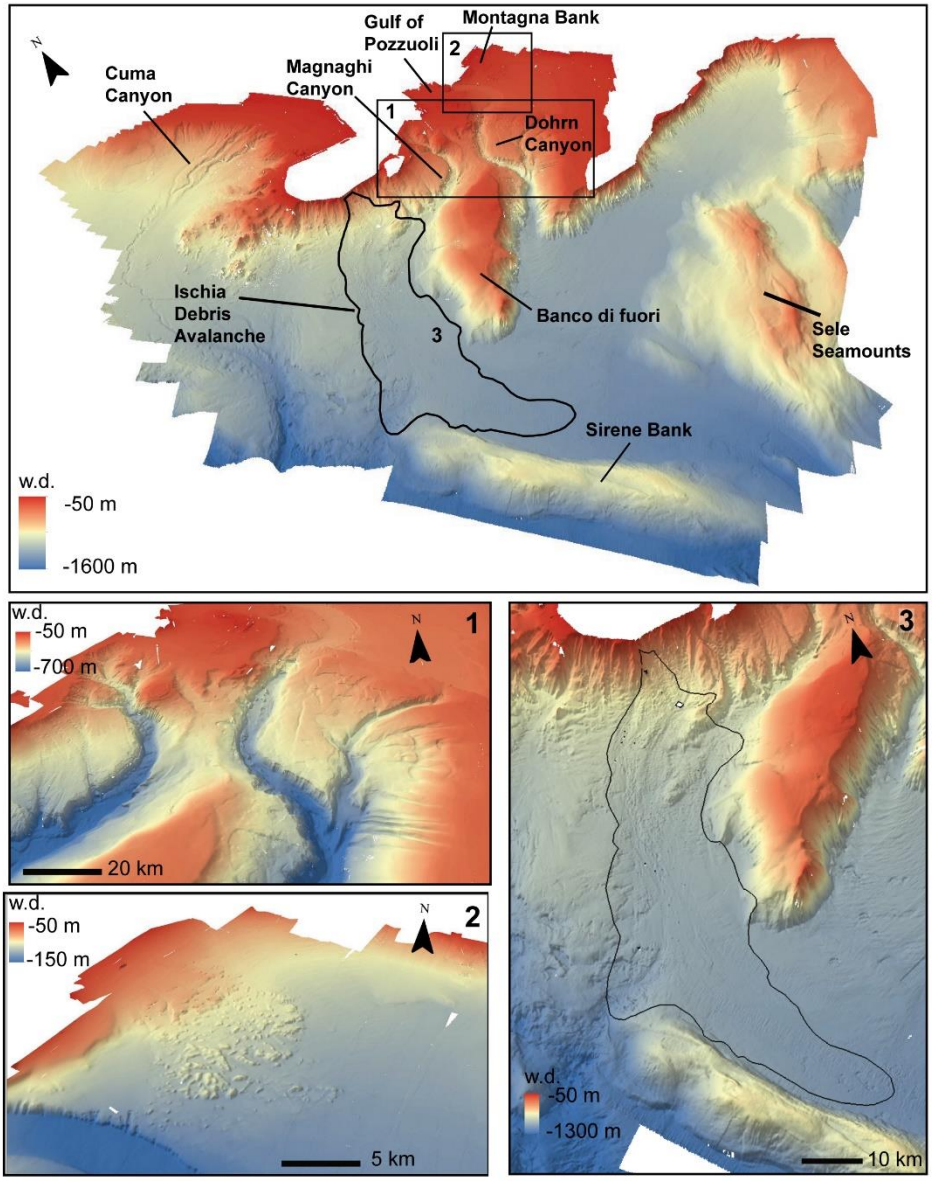

Figure 3. Bathymetric map of the study area (20 m resolution, 2 vertical exaggeration) showing the main seabed features; (1) multibeam bathymetry (20 m resolution, x 2 vertical exaggeration) of the Dohrn and Magnaghi canyon systems; (2) multibeam bathymetry of the Montagna Bank area; and (3) multibeam bathymetry of the debris avalanche offshore the Ischia Island.

Coupled with other indices, this high-resolution bathymetry not only is valuable information to study sediment dynamics, and morphotectonics of canyons, structural highs and seamounts, but also represents a baseline to investigate the presence and distribution of benthic habitats and infer hydrological transients at the sea floor. To demonstrate how the newly acquired data allow to appreciate the variations of the seafloor, broad- and fine-scale BPI were calculated from the bathymetry in three selected sectors of the study area using the parameters reported in Table 5.

Table 5. Inner and outer radius used for calculation of Bathymetric Position Index (BPI) for selected areas by depth range.

Area	**Depth range (m)**	**Resolution (m)**	**Broad-scale BPI Inner – outer radius (cells)**	**Fine-scale BPI Inner – outer radius (cells)**
Canyons of the Gulf of Naples	50-100	2	30-60	2-5
	101-200	5	12-30	2-5
	201-500	10	6-15	2-5
	501-700	15	4-9	2-5
	701-1000	20	3-8	2-5
	1001-2500	30	2-5	2-5
Montagna Bank	50-100	2	30-60	5-8
	101-200	5	12-30	5-8
	201-500	10	6-15	5-8
Ischia debris avalanche	50-100	2	30-60	1-3
	101-200	5	12-30	1-3
	201-500	10	6-15	1-3
	501-700	15	4-9	1-3
	701-1000	20	3-8	1-3
	1001-1900	30	2-5	1-3

4.1.1 Canyons of the Gulf of Naples

The morphology of the Dohrn and Magnaghi Canyons is possibly controlled by the presence of extensional faults coupled with the volcanic activity characterising the area. Both canyons acted as large drainage systems within this proximal marine area during the Late Quaternary (Aiello et al., 2020 and references therein). The two branches of Dohrn Canyon are about 500 m wide and show a V-shaped profile in the upper part and a U-shaped profile in the lower part, suggesting uniform sediment fill of the thalweg. The bathymetric derivatives confirm the complexity of these drainage patterns, related to the stratigraphy of the eroded terrains and to the recurrence and or competence of the flows flushing the two systems: straight gullies

characterise the flanks of Dohrn Canyon and normally do not indent the outer shelf, with the exception of the area NW of Capri (Fig. 4). Canyon Dohrn emanates from Ammontatura channel, on the inner shelf, a possibly active sediment conduit also during sea level rise and high stand conditions; Dohrn Canyon undercuts its secondary branch located north of Capri Island under-excavating its base by 50m. The straight gullies on the flanks of Dohrn Canyon are hanging above the canyon thalweg suggesting the activity of powerful flows along the axis of the canyon. Moreover, the fine-scale BPI highlights terrace rims along Dohrn Canyon flanks and slide scars with a slide deposit at their foot (Aiello et al., 2020), as well as the gullies with head scarps and along-slope small-scale sand splays located on the southern flank of Banco di Fuori. Dohrn Canyon shows a radial bedform field in its lower portion where the canyon broadens, and its floor decreases its gradient. Comparison with pre-existing data in this area suggests that the bedform field has not moved in the last two decades.

In contrast, Magnaghi Canyon is shorter, less deeply incised and not gullied on its flanks, possibly reflecting its lack of connection to a major source of sediment-laden flows. The right-hand side of the canyon shows short and straight incisions with marked bedforms hat appear reminiscent of cyclic steps (Kostic, 2011; Slootman and Cartigny, 2020) and can be clearly discerned on the slope map and on the BPI maps.

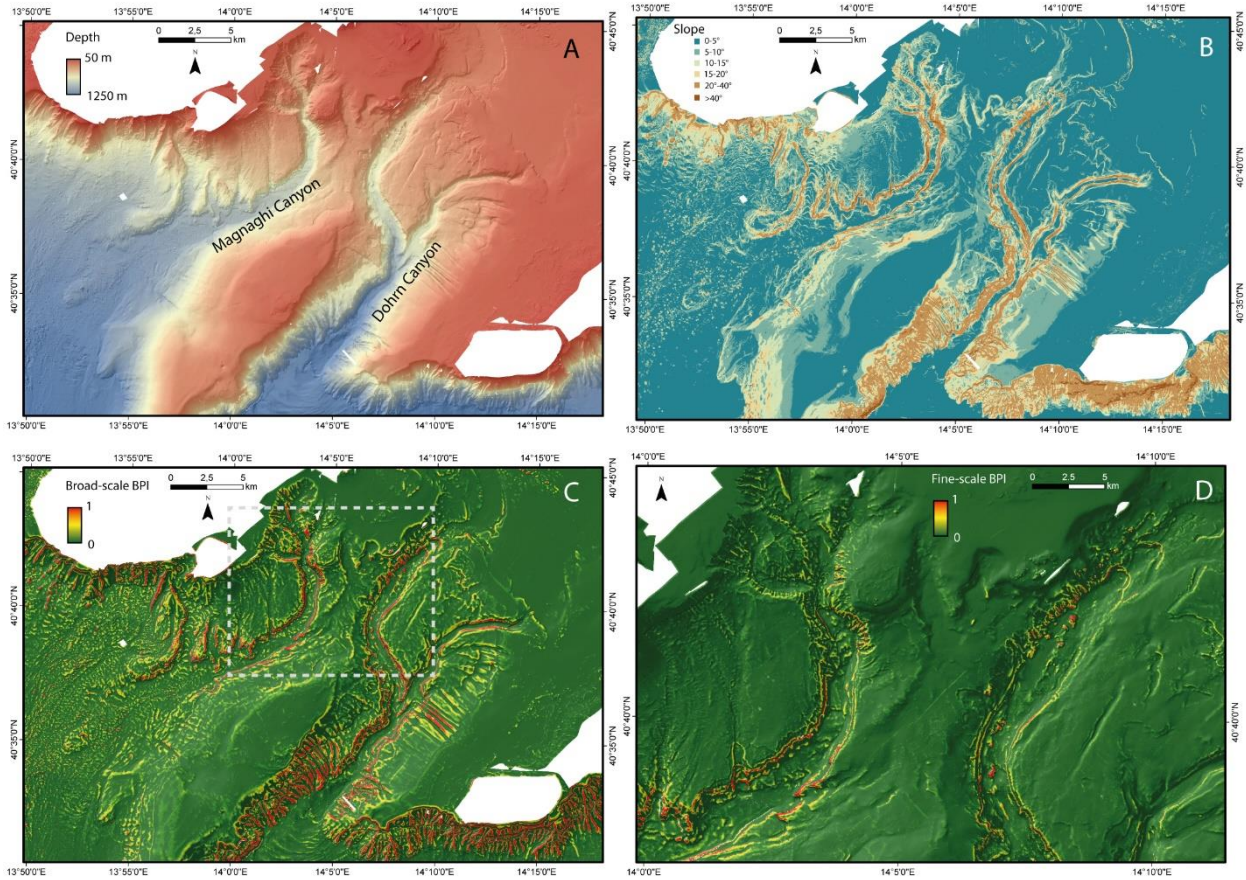

Figure 4 (A) Bathymetric data of canyons of the Gulf of Naples; (B) Slope; (C) positive values of broad-scale and (D) fine-scale BPI of a portion of the area (dashed rectangle in C) calculated from the newly acquired multi-resolution grid, showing the drainage pattern of the Dohrn and Magnaghi canyons.

4.1.2 Cuma Channel

Cuma Channel is a complex sediment conduit characterized by 1) an upper section, between the shelf-edge and the base of Gaeta basin, where three independent sub parallel channels present gullied heads, low sinuosity and flat channel floor; 2) a relatively narrow thalweg characterized by a prominent high sinuosity on the sub-horizontal floor of Gaeta Basin and 3) a straighter channel, proceeding in deeper waters across the steepening slope region.

Pairing both bathymetric and backscatter images prompt several questions that will be worth addressing in future cruises, after collecting complementary core and seismic-stratigraphy data. In particular:

1) there is no continuity between either of the three channels dissecting the upper slope and the high sinuosity channel on the floor of Gaeta basin; however, backscatter images hint to a seaward continuity of the most meridional of the three slope channels characterized by higher backscatter and, likely, coarser grained sediment. This channel reaches a north-south orientation before widening and rapidly reducing its seafloor reflectivity;

2) the high sinuosity to the west is therefore disconnected from its original feeder, upslope, and, proceeding downslope, bends gently to the Southeast and then to the Southwest in the lowermost tip of the mapped area; interestingly, the region located west of this gentle, multi-kilometric, bend is carved by several barchan-like scours that can be hypothetically ascribed to overflows of a much larger volume compared to the size of the channel conduit;

3) knowing that the Volturno prodelta has reached the shelf edge, it is possible that hyperpycnal flows from the river ignite flows on the slope that are capable to hug the seafloor and reshape its morphology, as documented during the modern sea level high stand in some other example of high discharge systems like the Crati River (Lucchi et al., 1983).

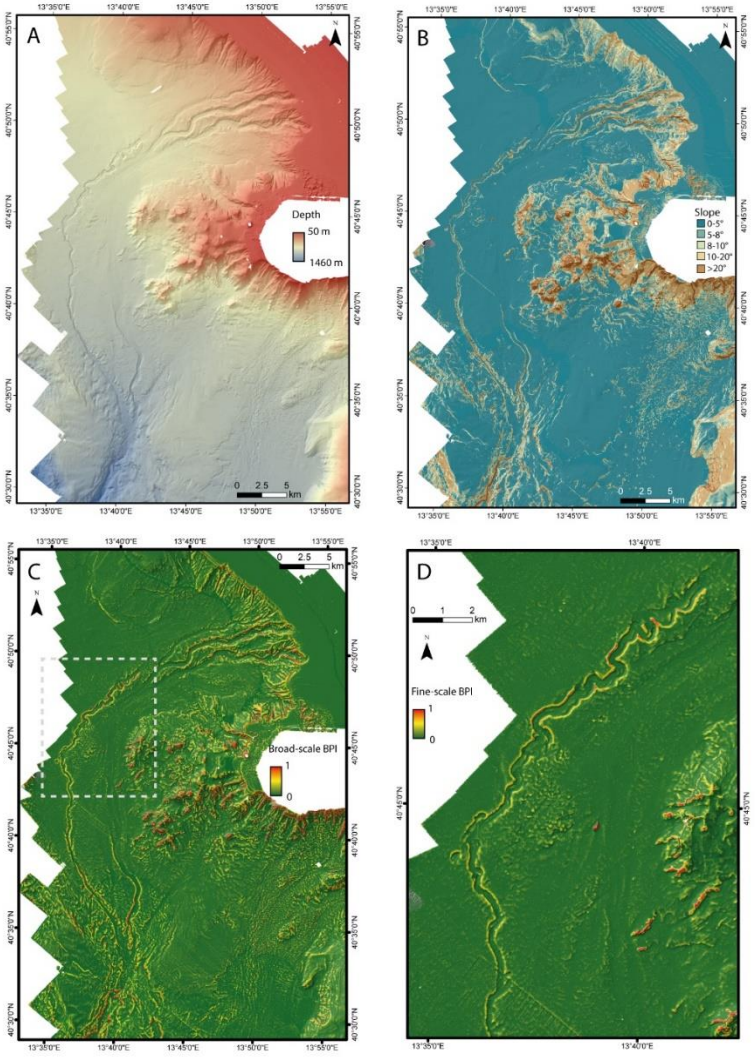

Figure 5 (A) Bathymetric data of the Cuma channel; (B) Slope; (C) positive values of broad-scale and (D) fine-scale BPI of a portion of the area (dashed rectangle in C) calculated from the newly acquired multi-resolution grid.

4.1.3 Montagna Bank

In the shallower area of the Gulf of Naples, **Montagna Bank** is a morphological high extending over 25 km^2 (Passaro et al. 2014, 2016, 2018; Ventura et al. 2016), where volcanoclastic materials (dominantly low-density pumice) underwent small-scale deformation leading to the growth of meter-scale sediment-diapirs and possible fluid-escape features; in particular, this hummocky area includes 280 mounds, 650 cones with meter-scale hight, and 30 pockmarks (Sacchi et al., 2019), between 100 and 150 m water depth. The slope calculated for the Montagna Bank shows the inclinations of both the whole morphological high and of the individual bedforms surrounding it (i.e., the flanks of the Ammontatura channel and sedimentary bedforms located W of the Montagna Bank). Furthermore, the calculated BPIs reveal large and small mounds constituting the hummocky-like morphology of the large-scale relief.

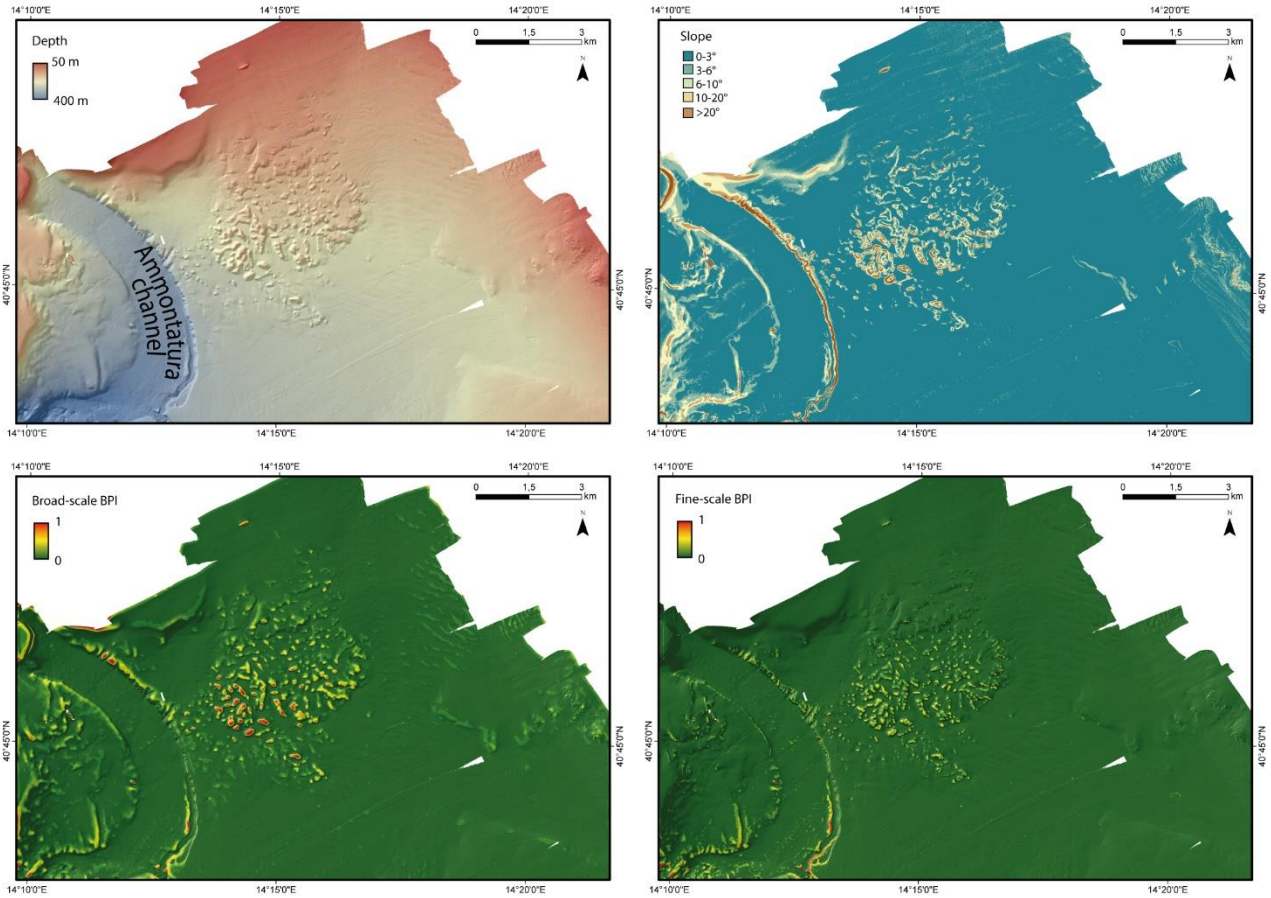

Figure 6. (A) Bathymetric data of the Montagna Bank; (B) Slope; (C) broad-scale and (D) fine-scale BPI calculated from the newly acquired multi-resolution grid, showing the morphology of the Montagna Bank.

4.1.4 Ischia debris avalanche

The Ischia debris-avalanche is located south of Ischia Island and is a 50-km-long tongue characterised by a hummocky topography extending for about 200 km^2 with fields of giant blocks spanning in size from a few metres to > 200 m across and with larger blocks being up to 30–50 m high (Chiocci and de Alteriis, 2006; de Alteriis et al., 2010). The hummocky deposit follows the local pre-collapse topography, and, on its eastern side, it overflows into the Magnaghi Canyon. The slope (Fig. 6B), the broad-scale (Fig. 6C), and fine-scale (Fig. 6D) BPI obtained using different inner and outer rays (Tab. 5), calculated from the newly acquired bathymetric data, allow to better appreciate the morphology of the deposits and clearly identify individual debris blocks, allowing better measurement of their size and volume.

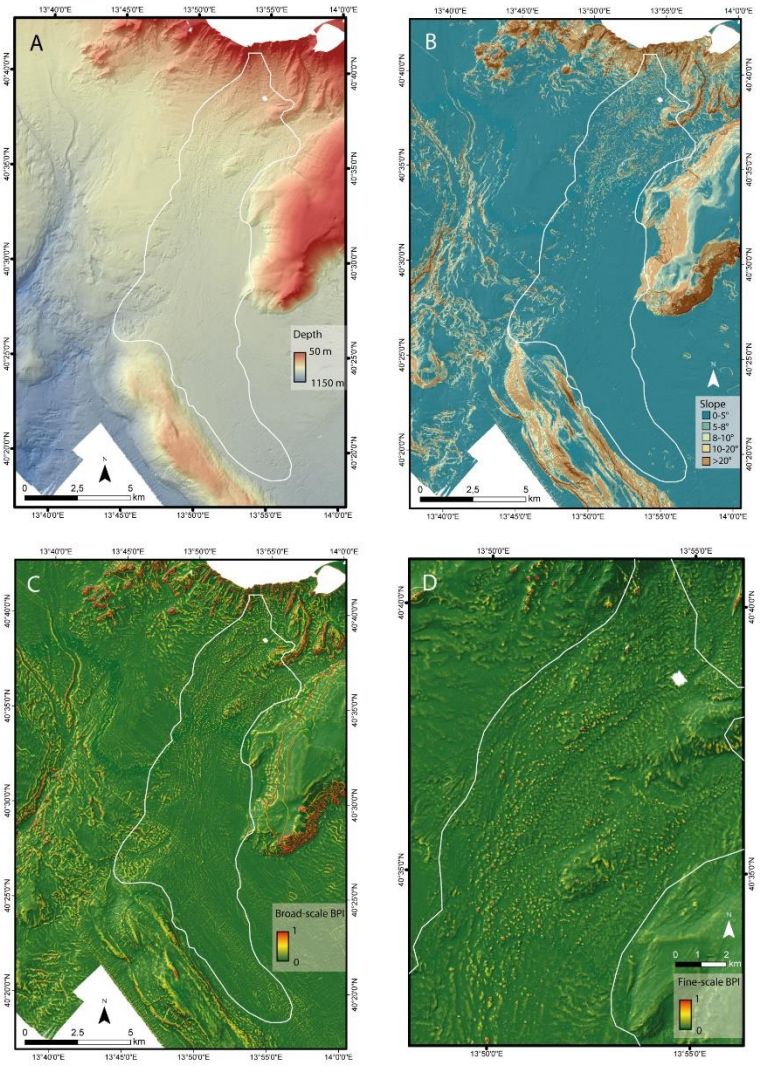

Figure 7. (A) Bathymetric data of the Ischia Debris Avalanche; (B) Slope; (C) broad-scale and (D) fine-scale BPI calculated from the newly acquired multi-resolution grid, showing the location and morphology of debris blocks. The white square delimitates the area that contains the debris avalanche.

4.2 The multi-grid backscatter mosaic

The backscatter intensity data acquired during the JammeGaia22 cruise represent the first dataset covering the entire Gulf of Naples, Ischia surroundings, Salerno Valley and Sirene Smt. Three mosaics were exported at different spatial resolutions: 5 m for the dataset acquired using the EM2040 system, 10 m for EM712 and 30 m for EM304 (Figure).

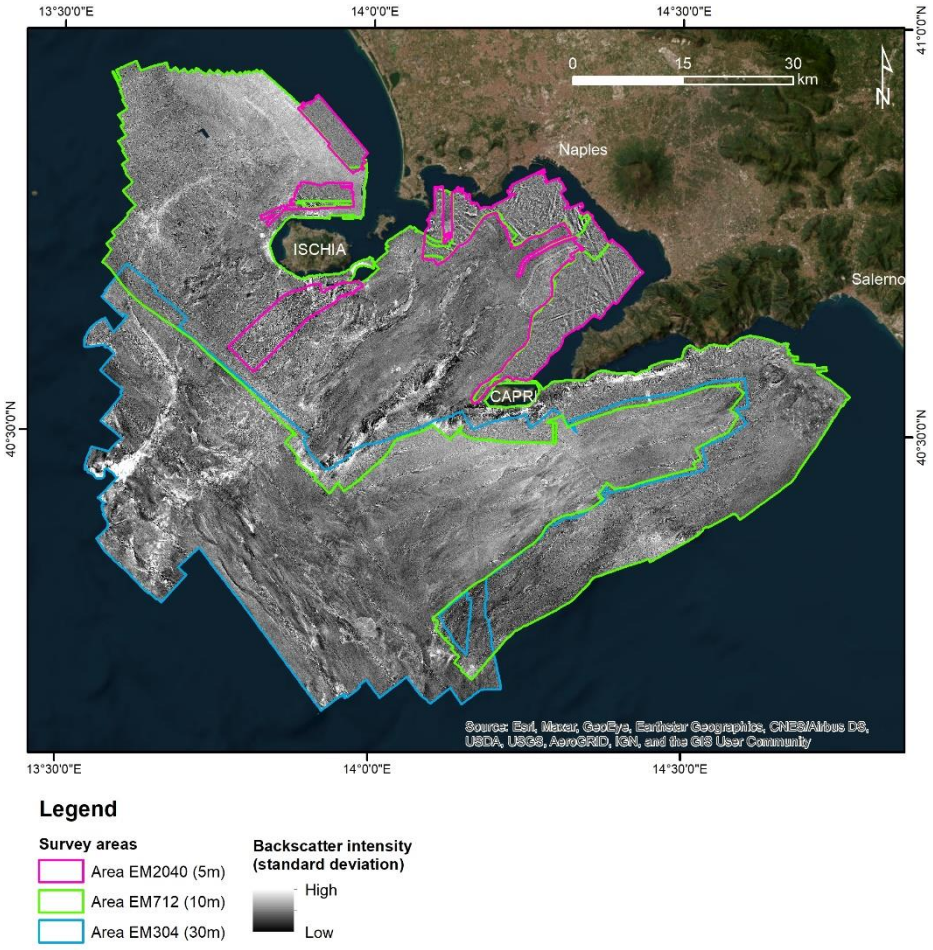

Figure 8. Backscatter mosaics acquired during the JammeGaia22 cruise with the survey areas covered by the three MBES.

Details are shown for four areas: Montagna Bank, Sorrento peninsula, north and west Ischia Island, and Magnaghi canyon head (Figure 8). The backscatter highlighted the hummocky-like morphology of the Montagna Bank and the trawl marks on the seabed around it. The backscatter dataset of the Sorrento peninsula revealed the occurrence of patterns likely associated with coralligenous bioconstructions (the lighter areas) and seagrass meadows along the coast, as previously highlighted in other studies (CARG - Geological CARtography project; EMODnet Seagrass cover (Essential Ocean Variable) in European waters (2023); Russo et al. 2008; Buonocore et al., 2020). Also, the hummocky morphology of the debris avalanches occurring north and west of Ischia Island is enhanced by the seabed reflectivity, together with features of fluid escapes (white spots in Figure 8C) around Ischia Island and in the head of the Magnaghi canyon, due to the hydrothermal activity characterizing the area.

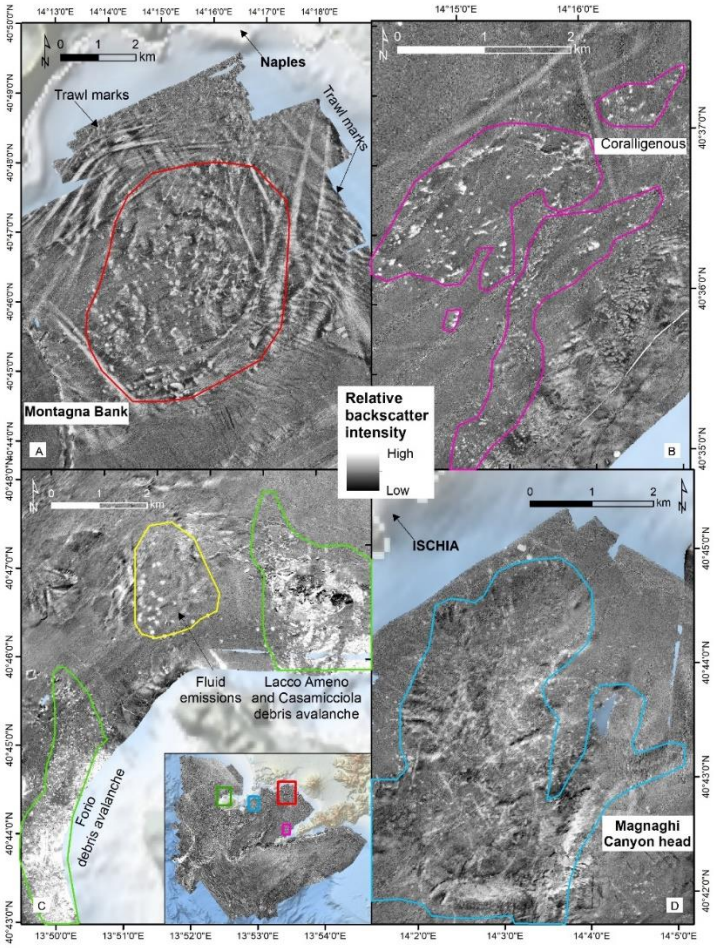

Figure 9. Details of the seabed backscatter in different locations: A) Montagna Bank hummocky morphology and trawl marks (EM2040 – 5m); B) Coralligenous bioconstructions west of the Sorrento peninsula (EM712 – 10m); C) debris avalanches north and west of Ischia Island and fluid escape features (EM712 – 10m); D) head of the Magnaghi Canyon characterized by fluid escape features, trawl marks and areas potentially hosting cold-water corals (EM712 – 10m).

4.3 MBES data quality

The uncertainty of the bathymetric data was calculated in Qimera v.2.5.4 according to the IHO Standards for Hydrographic Surveys 2-44 6th Edition, 2022. Total Horizontal Uncertainty (THU) and Total Vertical Uncertainty (TVU) were calculated considering the standard deviation offsets of the MRU, MBES, sound velocity probe, and positioning system. Parameters used for the calculation of THU and TVU were taken from the datasheet of the MBES systems and installation report (Table 6). The uncertainty values of EM2040 vary depending on the sampling frequency and depth changes during the survey. Hence, the values presented below are the range of uncertainty calculated for 200 kHz and 300 kHz and different pulse lengths that were used during acquisition.

Table 6. Parameters used to calculate Total Horizontal Uncertainty and Total Vertical Uncertainty

	EM2040	EM712	EM304
Echosounder			
Pulse Length	2, 3, 6, and 12 ms	2 ms	7.5 ms
Sampling Frequency	200kHz, 300 kHz,	70 kHz	25 kHz
Sound Velocity			
SD Surface sound speed	0.02 m/s	0.02 m/s	0.02 m/s
Beam Width			
Beam Width Along (Tx)	0.4°	0.5°	1.0°
Beam Width Across (Rx)	0.7°	1.0°	1.0°
Offsets (Argo)			
SD Roll Offset	0.04°	0.04°	0.04°
SD Pitch Offset	0.02°	0.02°	0.02°
SD Heading Offset	0.02°	0.02°	0.02°
POS			
SD Horizontal	0.1 m	0.1 m	0.1 m
SD Vertical	0.1 m	0.1 m	0.1 m

Although the scope of our survey was not related to navigation safety, we evaluated whether the horizontal uncertainty (THU) and vertical uncertainty (TVH) values met the IHO Standards for Hydrographic Surveys 2-44 6th Edition, 2022. Since we operated deep areas and the underkeel clearance was not an issue, THU and TVU were compared with the Maximum Allowable THU and TVU calculated at the minimum depth sampled for each MBES according to IHO Standards for Order 2 and 1b.

The results show the lowest horizontal uncertainty for data collected using EM2040 (THU = 1.66 to 4.94 m), while those collected with EM304 present the highest uncertainty (THU = 20.03 m) (

Table 7). The lowest vertical uncertainty was obtained for EM712 (TVU= 1.29 m), whilst the highest for EM2040 (TVU = 4.77 m).

The estimated THUs and TVUs of EM712 and EM304 were below their Maximum Allowable values for both Orders 2 and 1. The TVU calculated for the EM2040 is above its Maximum Allowable value for Orders 2 and 1. However, the quality of the data acquired was high enough to produce high-resolution bathymetry and for the scopes of our survey.

Table 7. Mean horizontal and vertical uncertainties of bathymetric data collected using different multibeam systems, and the accepted IHO error limits, which shows that the data collected are within the IHO standards.

	THU (m)	TVU (m)	Order 2 Maximum Allowable THU (m)	Order 1 Maximum Allowable THU (m)	Order 2 Maximum Allowable TVU (m)	Order 1 Maximum Allowable TVU (m)
EM2040	1.66 - 4.94	0.88 - 4.77	25 at 50m	7.5 at 50m	1.52 at 50m	0.82 at 50m
EM712	8.98	1.29	35 at 150m	12.5 at 150m	3.29 at 150m	2.01 at 150m
EM304	20.03	3.67	120 at 1000m	55 at 1000m	23.02 at 1000m	13.01 at 1000m

The uncertainty values calculated for JammeGaia22 survey data testify that the seafloor map of the Gulf of Naples obtained with the new technologies installed on board the R/V Gaia Blu represents a product of high quality. This new dataset will serve as a crucial baseline for future in-depth analysis of the geomorphology of the area, favoring the identification of seabed features at unprecedented resolution.

A significant improvement in the resolution of the data appears evident when comparing the morphology of the Ischia debris avalanche from DTM at 20 m horizontal resolution generated from the ancient and modern datasets. The newly acquired dataset shows better coverage and less noise than the 2001 dataset (Figure 9). The blocks of the landslide deposit can be also clearly identified in the new dataset whilst the identification is not obvious for some areas in the 2001 dataset.

To test if this increase in the resolution has an impact on geomorphological indices derived from the bathymetry, we calculated the fine-scale BPI from the 20 m-resolution DTMs (2001 and the JammeGaia22 surveys) using the same parameters for both the datasets, reported in Table 5. The results show a much higher noise level for the 2001 DTM with respect to the JammeGaia22 dataset (Figure 10). The noise was higher especially at the overlap among the swaths on the western part of the dataset, and the central beams of the swath in the central part of the data, where most of the landslide blocks occur. Such blocks are better detected and isolated through BPIs in 2022 DTM, rather than in 2001 DTM.

4.4 Comparison to previous data

The area for this study was selected not only for its intriguing dynamic, tectonic and volcanic activity, benthic boundary processes and seafloor biodiversity, and widespread human impacts of various origins. An additional reason was offered by the opportunity to compare the newly acquired data with a previous high-standard multibeam study of the area. In fact, this area has been already mapped since the late ‘90s with state of the art (for that time) instrumentation and presented in extremely accurate 3D views (D’Argenio et al., 2004; de Alteriis et al., 2010; Passaro et al., 2014; Sacchi et al., 2014; Budillon et al., 2016; Paoletti et al., 2016; Passaro et al., 2016a, 2016b; Di Martino et al., 2021; Aiello and Sacchi, 2022). The limitation of

that original database came from the need to acquire the data in a succession of surveys spanning several years and using instruments with rather variable resolutions. Nevertheless, also thanks to the extreme accuracy of the data processing performed at that time, this 20-year-old database provided an excellent basis for comparison with the newly acquired, more homogenous, database. Of course, the comparison cannot be pushed to the highest resolution offered by the modern instruments on Gaia Blu but, even on lower resolution, the comparison among 20 m grids from the two data sets can be extremely valuable.

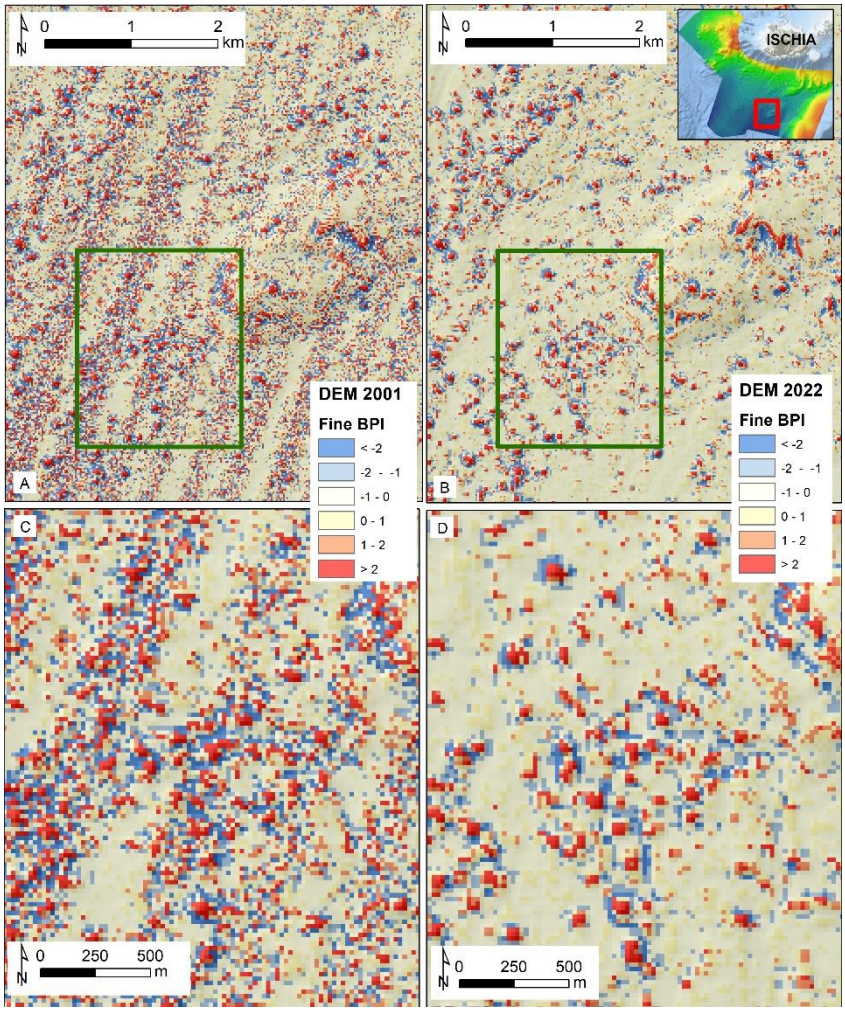

Figure 10. Fine-scale BPI calculated on the 2001 DTM (A) and JammeGaia22 DTM (B) for the area of the Ischia debris avalanche; noticeably, the 2001 dataset is very noisy. Detail of the blocks accumulation for 2001 DTM (C) and JammeGaia22 DTM (D): despite both datasets have same spatial resolution (20 m), the newly acquired dataset allows to better discriminate and map blocks.

5. **Data availability**

All datasets, products and web services are managed through the ISMAR Marine Spatial Data Infrastructure – MSDI (Foglini & Grande 2023) and follow the ISMAR-CNR Data policy (https://doi.org/10.26383/CNR-ISMAR.2023.6). Bathymetric datasets gathered by the MBES in the format GSF (generic sensor format), and bathymetric and backscatter surfaces (GeoTIFF) are shared in the Marine Geoscience Data System (MGDS) (Table 8).

Data are also available as Web Map Services (WMS), that are interoperable with other infrastructures and permit the integration of the spatial data in other geoportals or directly in a desktop environment (e.g., QGIS, ArcMap). Data are freely accessible thought two main interfaces: the metadata catalogue and the WebGIS.

The CNR-ISMAR GeoNetwork metadata catalogue ((http://seamap-catalog.data.ismar.cnr.it:8080/geonetwork) allows users to find the JammeGaia22 products (refer to Table 8 for direct links to products),containing information about access and use policy, link to download the data, how to cite the data, DOI, and links to external repositories (such as EMODnet and MGDS).

The WebGIS (http://seamap-explorer.data.ismar.cnr.it:8080/mokaApp/applicazioni/ismarBoApp) publishes survey areas, multibeam navigation lines, bathymetric surfaces and backscatter mosaics. Users can navigate the map to the JammeGaia22 survey area, explore the layer list and open the geophysical data and products. By clicking on spatial objects on the map, users can access the related information, such as the download link.

Table 8. Products of the JammeGaia22 oceanographic cruise with relative link.

Product	Typology	Depth range	Spatial resolution	Format	Link CNR-ISMAR Catalog	DOIs
Survey JAMME GAIA 2022	Cruise report	-	-	PDF	http://libeccio.bo.ismar.cnr.it:8080/geonetwork/srv/eng/catalog.search#/metadata/6cd1080c-f41f-4c9d-907b-297d25f554e5	Foglini, et al., 2024a, https://doi.org/10.26383/CNR-ISMAR.2024.4
JG22_SwathLines_EM2040	MBES processed lines	-	-	GSF	http://libeccio.bo.ismar.cnr.it:8080/geonetwork/srv/eng/catalog.search#/metadata/6213658d-ca9a-4e40-af07-e4f7b329203a	Foglini, 2024a http://dx.doi.org/10.60521/331589
JG22_SwathLines_EM712	MBES processed lines	-	-	GSF	http://libeccio.bo.ismar.cnr.it:8080/geonetwork/srv/eng/catalog.search#/metadata/62136	Foglini 2024b

					58d-ca9a-4e40-af07-e4f7b329203a	http://dx.doi.org/10.60521/331587
JG22_SwathLines_EM304	MBES processed lines	-	-	GSF	http://libeccio.bo.ismar.cnr.it:8080/geonetwork/srv/eng/catalog.search#/metadata/6213658d-ca9a-4e40-af07-e4f7b329203a	Foglini 2024c, http://dx.doi.org/10.60521/331584
JG22_50_120_2m	Bathymetric surface	50-120 m	2 m	ASCII GeoTIFF ESRI_grid	http://libeccio.bo.ismar.cnr.it:8080/geonetwork/srv/eng/catalog.search#/metadata/927334e6-021a-4eed-a0a6-f209df3b17ad	Foglini et al. 2024b, http://dx.doi.org/10.60521/331667
JG22_100_200_5m	Bathymetric surface	100 -200 m	5 m	ASCII GeoTIF ESRI_grid	http://libeccio.bo.ismar.cnr.it:8080/geonetwork/srv/eng/catalog.search#/metadata/5e384b50-ea4d-4e68-b023-d5b64ebd5ed8	
JG22_180_500_10m	Bathymetric surface	180-500 m	10 m	ASCII GeoTIFF ESRI_grid	http://libeccio.bo.ismar.cnr.it:8080/geonetwork/srv/eng/catalog.search#/metadata/e956cee4-ba1c-41b7-932b-4031932c9a9d	
JG22_480_700_15m	Bathymetric surface	480-700 m	15 m	ASCII GeoTIFF ESRI_grid	http://libeccio.bo.ismar.cnr.it:8080/geonetwork/srv/eng/catalog.search#/metadata/5124f1d9-982c-4996-8333-298eb62e5c73	
JG22_680_1000_20m	Bathymetric surface	680-1000 m	20 m	ASCII GeoTIFF ESRI_grid	http://libeccio.bo.ismar.cnr.it:8080/geonetwork/srv/eng/catalog.search#/metadata/21481	

					1a5-1700-413f-9b3f-95d2ddd29996	
JG22_980_1300_30m	Bathymetric surface	980-1300 m	30 m	ASCII GeoTIFF ESRI_grid	http://libeccio.bo.ismar.cnr.it:8080/geonetwork/srv/eng/catalog.search#/metadata/a43cf1d4-abc6-43e4-9f66-fac08827c5dd	
JG22_1280_2120_40m	Bathymetric surface	1280-2120 m	40 m	ASCII GeoTIFF ESRI_grid	http://libeccio.bo.ismar.cnr.it:8080/geonetwork/srv/eng/catalog.search#/metadata/96388cc5-2c58-4ba3-9816-7231c69d96e8	
JG22_2040_5m	Backscatter mosaic from EM2040	-	5 m	ASCII GeoTIFF ESRI_grid	http://libeccio.bo.ismar.cnr.it:8080/geonetwork/srv/eng/catalog.search#/metadata/6ec52054-ac6c-46e6-966b-8a88d1cf4351	Foglini et al. 2024c, http://dx.doi.org/10.60521/331668
JG22_712_10m	Backscatter mosaic from EM712	-	10 m	ASCII GeoTIFF ESRI_grid	http://libeccio.bo.ismar.cnr.it:8080/geonetwork/srv/eng/catalog.search#/metadata/d4c1635f-69f2-4ebc-9174-d2a9d60a1e58	
JG22_304_30m	Backscatter mosaic from EM304	-	30 m	ASCII GeoTIFF ESRI_grid	http://libeccio.bo.ismar.cnr.it:8080/geonetwork/srv/eng/catalog.search#/metadata/94f61db5-c186-48a6-b82b-7d9685c2a541	

6. Conclusions

The JammeGaia22 cruise led to the creation of DTM and backscatter mosaics at different resolutions for the Gulf of Naples, by using three different state-of-the-art MBESs. The dataset has been obtained through a reproducible processing workflow and corresponds to a major upgrade of a pre-existing bathymetry of the area. The vertical and positioning uncertainties of the bathymetric data fall within the IHO standards and satisfy Order 1b for EM2040 and Order 2 for EM712 and EM304.

The newly acquired multi beam maps reveal submerged morphologies at a scale and resolution never achieved before for the study area, allowing for a wide range of local and regional studies, spanning from geological and geomorphological research to marine habitat mapping and sea-floor monitoring. Furthermore, these high-resolution bathymetry and backscatter datasets can be useful for many and diverse applications, such as maritime spatial planning and for designing innovative conservation strategies.

The new data base is released to the community as a benchmark reference against which future sea-floor changes can be quantified and ascribed to either the activity of subaqueous volcanic apparatuses, in particular in the vicinity of the Flegraean Field, the flux of density flows along major conduits like Cuma Channel, and Magnaghi and Dohrn Canyons, slope instability leading to mass-transport deposits or sand splays at the mouth of slope gullies. Large scale bedforms are particularly developed in regions flow rearrangement like in a bend of Cuma Channel, west of Ischia Island, or in the area of possible cyclic steps, on the slope south of Ischia. Backscatter data help recognizing areas of potential occurrence of cold-water coral colonies and coralligenous bioconstructions, a key element of the Mediterranean biodiversity richness. Finally, both bathymetric and backscatter data help define the areas most impacted by fish trawling, smoothing and remoulding the seafloor, fluid escape features and landslides.

7. Author contribution

FF: Supervisor, data collection and processing, conceptualisation, and writing; MR: Supervisor, data collection, conceptualisation; RT: Supervisor, data collection and processing; GC, DG: data collection, data processing, first draft writing; VG, MP: data management, data processing, first draft writing; LP, CP, FB, FM, MC, MS, ML, PM data collection and review; GD, SI, ANT, AP, AM, AR data collection and processing; FT: Supervisor and review.

8. Competing interests

The contact author has declared that none of the authors has any competing interests.

9. Acknowledgements

We thank captain, crew, and scientific staff of R/V Gaia Blu for their skilful and efficient cooperation during operations at sea.

This is ISMAR-Bologna scientific contribution no. 2088.

References

Aiello, G., Iorio, M., Molisso, F., and Sacchi, M.: Integrated Morpho-Bathymetric, Seismic-Stratigraphic, and Sedimentological Data on the Dohrn Canyon (Naples Bay, Southern Tyrrhenian Sea): Relationships with Volcanism and Tectonics, Geosciences, 10, 319, https://doi.org/10.3390/geosciences10080319, 2020.

Aiello, G., Sacchi, M.: New morpho-bathymetric data on marine hazard in the offshore of Gulf of Naples (Southern Italy). *Natural Hazards* 111(3), 2881-2908, 2022.

Albert, P. G., Giaccio, B., Isaia, R., Costa, A., Niespolo, E. M., Nomade, S., Pereira, A., Renne, P. R., Hinchliffe, A., Mark, D. F., Brown, R. J., and Smith, V. C.: Evidence for a large-magnitude eruption from Campi Flegrei caldera (Italy) at 29 ka, *Geology*, 47, 595–599, https://doi.org/10.1130/G45805.1, 2019.

Amato, V., Aucelli, P. P. C., Cinque, A., D'Argenio, B., Donato, V. D., Pappone, G., Petrosino, P., Rosskopf, C. M., and Ermolli, E. R.: Holocene palaeo-geographical evolution of the Sele river coastal plain (Southern Italy): new morpho-sedimentary data from the Paestum area, *Alpine and Mediterranean Quaternary*, 24, 5–7, 2011.

Angiolillo, M., Bo, M., Toma, M., Giusti, M., Salvati, E., Giova, A., Lagudi, A., Rossi, L., Collina, M., Bruno, F., Canese, S., and Tunesi, L.: A baseline for the monitoring of Mediterranean upper bathyal biogenic reefs within the marine strategy framework directive objectives, Deep Sea Research Part I: Oceanographic Research Papers, 194, 103963, https://doi.org/10.1016/j.dsr.2023.103963, 2023.

Appolloni, L., Sandulli, R., Vetrano, G., and Russo, G. F.: A new approach to assess marine opportunity costs and monetary values-in-use for spatial planning and conservation; the case study of Gulf of Naples, Mediterranean Sea, Italy, Ocean & Coastal Management, 152, 135–144, https://doi.org/10.1016/j.ocecoaman.2017.11.023, 2018.

Appolloni, L., Zeppilli, D., Donnarumma, L., Baldrighi, E., Chianese, E., Russo, G., and Sandulli, R.: Seawater Acidification Affects Beta-Diversity of Benthic Communities at a Shallow Hydrothermal Vent in a Mediterranean Marine Protected Area (Underwater Archaeological Park of Baia, Naples, Italy), Diversity, 12, 464, https://doi.org/10.3390/d12120464, 2020.

Basterretxea, G., Font-Muñoz, J. S., Salgado-Hernanz, P. M., Arrieta, J., and Hernández-Carrasco, I.: Patterns of chlorophyll interannual variability in Mediterranean biogeographical regions, Remote Sensing of Environment, 215, 7–17, https://doi.org/10.1016/j.rse.2018.05.027, 2018.

Bavestrello, G., Bo, M., Canese, S., Sandulli, R., and Cattaneo-Vietti, R.: The red coral populations of the gulfs of Naples and Salerno: human impact and deep mass mortalities, Italian Journal of Zoology, 81, 552–563, https://doi.org/10.1080/11250003.2014.950349, 2014.

Beaudoin, J., Renoud, W., Mohammadloo, T. H., & Snellen, M. Automated correction of refraction residuals. In HYDRO18 conference, 2018.

Bellucci, F., Milia, A., Rolandi, G., and Torrente, M. M.: Chapter 8 Structural control on the Upper Pleistocene ignimbrite eruptions in the Neapolitan area (Italy): volcano tectonic faults versus caldera faults, in: Developments in Volcanology, vol. 9, edited by: De Vivo, B., Elsevier, 163–180, https://doi.org/10.1016/S1871-644X(06)80022-7, 2006.

Bianchi, C. N. and Morri, C.: Marine Biodiversity of the Mediterranean Sea: Situation, Problems and Prospects for Future Research, Marine Pollution Bulletin, 40, 367–376, https://doi.org/10.1016/S0025-326X(00)00027-8, 2000.

Budillon, F., Violante, C., De Lauro M. I fondali delle Isole Flegree, morfologia e geologia. in: Ambiente marino costiero e territorio delle isole flegree (Ischia Procida e Vivara – Golfo di Napoli). Risultati di uno studio multidisciplinare, edited by: Gambi, M. C., De Lauro, M., Jannuzzi, F., Mem. Acc. Sci. Fis. E Matem., Napoli 5, 45-66, 2003.

Budillon, F., Cesarano, M., Conforti, A., Pappone, G., Di Martino, G., Pelosi, N.: Recurrent superficial sediment failure and deep gravitational deformation in a Pleistocene slope marine succession: The Poseidonia slide (Salerno Bay, Tyrrhenian Sea), Submarine Mass Movements and Their Consequences, 6th International Symposium, 273-283, 2016.

Budillon F., Firetto Carlino M., Innangi S., Passaro S., Tonielli R., Trincardi F., Sprovieri M.: The Anthropogenic Footprint of Physical Harm on the Seabed of Augusta Bay (Western Ionian Sea). Journal of Marine Science and Engineering 10 (11), 1737.Buonocore, E., Appolloni, L., Russo, G. F., and Franzese, P. P.: Assessing natural capital value in marine ecosystems through an environmental accounting model: A case study in Southern Italy, Ecological Modelling, 419, 108958, https://doi.org/10.1016/j.ecolmodel.2020.108958, 2020.

Burrough, P. A., and McDonell, R. A: Principles of Geographical Information Systems, Oxford University Press, New York, 120 pp., 1998.

Canals, M., Pham, C. K., Bergmann, M., Gutow, L., Hanke, G., Sebille, E. van, Angiolillo, M., Buhl-Mortensen, L., Cau, A., Ioakeimidis, C., Kammann, U., Lundsten, L., Papatheodorou, G., Purser, A., Sanchez-Vidal, A., Schulz, M., Vinci, M., Chiba, S., Galgani, F., Langenkämper, D., Möller, T., Nattkemper, T. W., Ruiz, M., Suikkanen, S., Woodall, L., Fakiris, E., Jack, M. E. M., and Giorgetti, A.: The quest for seafloor macrolitter: a critical review of background knowledge, current methods and future prospects, Environ. Res. Lett., 16, 023001, https://doi.org/10.1088/1748-9326/abc6d4, 2021.

CARG (Geological CARtography) project: https://www.isprambiente.gov.it/en/projects/soil-and-territory/carg-project-geologic-and-geothematic-cartography (last access: 28 February 2024)

Chiocci, F. L. and De Alteriis, G.: The Ischia debris avalanche: first clear submarine evidence in the Mediterranean of a volcanic island prehistorical collapse, Terra Nova, 18, 202–209, https://doi.org/10.1111/j.1365-3121.2006.00680.x, 2006.

Coll, M., Piroddi, C., Albouy, C., Ben Rais Lasram, F., Cheung, W. W. L., Christensen, V., Karpouzi, V. S., Guilhaumon, F., Mouillot, D., Paleczny, M., Palomares, M. L., Steenbeek, J., Trujillo, P., Watson, R., and Pauly, D.: The Mediterranean Sea under siege: spatial overlap between marine biodiversity, cumulative threats and marine reserves, Global Ecology and Biogeography, 21, 465–480, https://doi.org/10.1111/j.1466-8238.2011.00697.x, 2012.

549 D'Argenio, B., Angelino, A., Aiello, G., de Alteriis, G., Milia, A., Sacchi, M., Tonielli, R., Budillon, F., Chiocci,
550 F. L., Conforti, A., Lauro, M., Di Martino, G., D'Isanto, C., Esposito, E., Ferraro, L., Innangi, S., Insinga, D. D.,
551 Iorio, Marsella, E., Molisso, F., Morra, V. B., Passaro, S., Pelosi, N., Pordo, S., Raspini, A., Ruggeri, S.,
552 Sarnacchiaro, G., Terranova, C., Vilardo, G., and Violante, C.: Digital elevation model of the Naples Bay and
553 adjacent areas (Eastern Tyrrhenian Sea), in: Mapping Geology in Italy, Atlante di Cartografia Geologica, vol.
554 Convegno Internazionale Firenze, edited by: Pasquarè, E. and Venturini, G., Firenze, Italy, 21–28, 2004.

555 de Alteriis, G., Insinga, D. D., Morabito, S., Morra, V., Chiocci, F. L., Terrasi, F., Lubritto, C., Di Benedetto, C.,
556 and Pazzanese, M.: Age of submarine debris avalanches and tephrostratigraphy offshore Ischia Island, Tyrrhenian
557 Sea, Italy, Marine Geology, 278, 1–18, https://doi.org/10.1016/j.margeo.2010.08.004, 2010.

558 Deino, A. L., Orsi, G., de Vita, S., and Piochi, M.: The age of the Neapolitan Yellow Tuff caldera-forming eruption
559 (Campi Flegrei caldera – Italy) assessed by 40Ar/39Ar dating method, Journal of Volcanology and Geothermal
560 Research, 133, 157–170, https://doi.org/10.1016/S0377-0273(03)00396-2, 2004.

561 Díaz, S., Settele, J., Brondízio, E. S., Ngo, H. T., Agard, J., Arneth, A., Balvanera, P., Brauman, K. A., Butchart,
562 S. H. M., Chan, K. M. A., Garibaldi, L. A., Ichii, K., Liu, J., Subramanian, S. M., Midgley, G. F., Miloslavich, P.,
563 Molnár, Z., Obura, D., Pfaff, A., Polasky, S., Purvis, A., Razzaque, J., Reyers, B., Chowdhury, R. R., Shin, Y.-J.,
564 Visseren-Hamakers, I., Willis, K. J., and Zayas, C. N.: Pervasive human-driven decline of life on Earth points to
565 the need for transformative change, Science, 366, eaax3100, https://doi.org/10.1126/science.aax3100, 2019.

566 Di Martino, G., Innangi, S., Sacchi, M., Tonielli, R.: Seafloor morphology changes in the inner-shelf area of the
567 Pozzuoli Bay, Eastern Tyrrhenian Sea, Marine Geophysical Research, 42(2),13, 2021.

568 Dolan, M. F. J.: Calculation of slope angle from bathymetry data using GIS - effects of computation algorithm,
569 data resolution and analysis scale, Geological Survey of Norway Report No. 2012.041, 40 pp., 2012

570 Donnarumma, L., Appolloni, L., Chianese, E., Bruno, R., Baldrighi, E., Guglielmo, R., Russo, G. F., Zeppilli, D.,
571 and Sandulli, R.: Environmental and Benthic Community Patterns of the Shallow Hydrothermal Area of Secca
572 Delle Fumose (Baia, Naples, Italy), Front. Mar. Sci., 6, 685, https://doi.org/10.3389/fmars.2019.00685, 2019.

573 EMODnet Seagrass cover (Essential Ocean Variable) in European waters (2023):
574 https://emodnet.ec.europa.eu/geonetwork/emodnet/eng/catalog.search#/metadata/39746d9c-4220-425c-bc26-
575 7cb3056c36a5 (last access: 28 February 2024).

576 Foglini, F. Processed EM2040 Acoustic Backscatter and Swath Bathymetry data from R/V Gaia Blu cruise Jamme
577 Gaia22 (2022). MGDS. 2024a, doi:10.60521/331589

578 Foglini, F. Processed EM712 Acoustic Backscatter and Swath Bathymetry data from R/V Gaia Blu cruise Jamme
579 Gaia22 (2022). MGDS. 2024b, doi:10.60521/331587

580 Foglini, F. Processed EM304 Acoustic Backscatter and Swath Bathymetry data from R/V Gaia Blu cruise Jamme
581 Gaia22 (2022). MGDS. 2024c, doi:10.60521/331584

582 Foglini, F. and Grande, V.: A Marine Spatial Data Infrastructure to manage multidisciplinary, inhomogeneous and
583 fragmented geodata in a FAIR perspective ... the Adriatic Sea experience, Oceanologia, 65, 260–277,
584 https://doi.org/10.1016/j.oceano.2022.11.002, 2023.

585 Foglini, F., Tonielli, R., and Rovere M. Cruise report Survey JAMME GAIA 2022. CNR-ISMAR, 2024a,
586 https://doi.org/10.26383/CNR-ISMAR.2024.4

587 Foglini, F.; Tonielli, R. and M. Rovere. Multi-Resolution bathymetry grids of the Naples and Pozzuoli Gulf and
588 the Amalfi Coastal Area collected during cruise Jamme_Gaia22, 2022. MGDS. 2024b, doi:10.60521/331667

589 Foglini, F.; Tonielli, R. and M. Rovere. Multi-Resolution backscatter grids of the Naples and Pozzuoli Gulf and
590 the Amalfi Coastal Area collected during cruise Jamme_Gaia22, 2022. MGDS, 2024c,
591 doi:10.60521/331668Giaccio, B., Isaia, R., Fedele, F. G., Di Canzio, E., Hoffecker, J., Ronchitelli, A., Sinitsyn, A.
592 A., Anikovich, M., Lisitsyn, S. N., and Popov, V. V.: The Campanian Ignimbrite and Codola tephra layers: Two
593 temporal/stratigraphic markers for the Early Upper Palaeolithic in southern Italy and eastern Europe, Journal of
594 Volcanology and Geothermal Research, 177, 208–226, https://doi.org/10.1016/j.jvolgeores.2007.10.007, 2008.

595 Giaccio B., Hajdas I., Isaia R., Deino A., Nomade S. High-precision 14C and 40Ar/39Ar dating of the Campanian
596 Ignimbrite (Y-5) reconciles the time-scales of climatic-cultural processes at 40 ka. Sci. Rep. 7, 45940; doi:
597 10.1038/srep45940, 2017.

598 Iampietro, P. and Kvitek, R.: Iampietro, P., and R. Kvitek. 2002. Quantitative seafloor habitat classification using
599 GIS terrain analysis: Effects of data density, resolution, and scale. In Proceedings of the 22nd Annual ESRI User
600 Conference. San Diego, CA July 8–12, in: Proceedings of the 22nd Annual ESRI User Conference, 22nd Annual
601 ESRI User Conference, San Diego, CA, 2002.Isaia, R., Vitale, S., Marturano, A., Aiello, G., Barra, D., Ciarcia, S.,
602 Iannuzzi, E., and Tramparulo, F. D.: High-resolution geological investigations to reconstruct the long-term ground
603 movements in the last 15 kyr at Campi Flegrei caldera (southern Italy), Journal of Volcanology and Geothermal
604 Research, 385, 143–158, https://doi.org/10.1016/j.jvolgeores.2019.07.012, 2019.

605 Kastens, K., Mascle, J., Auroux, C., Bonatti, E., Broglia, C., Channell, J., Curzi, P., Emeis, K.-C., Glaçon, G.,
606 Hasegawa, S., Hieke, W., Mascle, G., McCoy, F., McKenzie, J., Mendelson, J., Müller, C., Réhault, J.-P.,
607 Robertson, A., Sartori, R., Sprovieri, R., and Torii, M.: ODP Leg 107 in the Tyrrhenian Sea: Insights into passive
608 margin and back-arc basin evolution, GSA Bulletin, 100, 1140–1156, https://doi.org/10.1130/0016-
609 7606(1988)100<1140:OLITTS>2.3.CO;2, 1988.

610 Kostic, S.: Modeling of submarine cyclic steps: controls on their formation, migration, and architecture. Geosphere,
611 7(2), 294-304, 2011.

612 Le Bas, T. P. RSOBIA: A new OBIA Toolbar and Toolbox in ArcMap 10.x for Segmentation and Classification,
613 in: Proceedings of GEOBIA 2016 : Solutions and synergies, 14-16 September 2016, Enschede, Netherlands, 6th
614 International Conference on Geographic Object-Based Image Analysis, GEOBIA 2016: Solutions & Synergies,
615 https://doi.org/10.3990/2.448, 2016.

616 Loreto, M. F., Zitellini, N., Ranero, C. R., Palmiotto, C., and Prada, M.: Extensional tectonics during the Tyrrhenian
617 back-arc basin formation and a new morpho-tectonic map, Basin Research, 33, 138–158,
618 https://doi.org/10.1111/bre.12458, 2021.

619 Lucchi, F. R., Colella, A., Gabbianelli, G., Rossi, S., & Normark, W. R.: The Crati submarine fan, Ionian sea. Geo-
620 marine letters, 3, 71-77, 1983.

Lundblad, E. R., Wright, D. J., Miller, J., Larkin, E. M., Rinehart, R., Naar, D. F., Donahue, B. T., Anderson, S. M., and Battista, T.: A Benthic Terrain Classification Scheme for American Samoa, Marine Geodesy, 29, 89–111, https://doi.org/10.1080/01490410600738021, 2006.

Lymer, G., Lofi, J., Gaullier, V., Maillard, A., Thinon, I., Sage, F., Chanier, F., and Vendeville, B. C.: The Western Tyrrhenian Sea revisited: New evidence for a rifted basin during the Messinian Salinity Crisis, Marine Geology, 398, 1–21, https://doi.org/10.1016/j.margeo.2017.12.009, 2018.

Madricardo, F., Foglini, F., Campiani, E., Grande, V., Catenacci, E., Petrizzo, A., Kruss, A., Toso, C., and Trincardi, F.: Assessing the human footprint on the sea-floor of coastal systems: the case of the Venice Lagoon, Italy, Sci Rep, 9, 6615, https://doi.org/10.1038/s41598-019-43027-7, 2019.

Marine Geoscience Data System – MGDS: https://www.marine-geo.org/ (last access: 28 February 2024).

Mattei, G., Rizzo, A., Anfuso, G., Aucelli, P. P. C., and Gracia, F. J.: A tool for evaluating the archaeological heritage vulnerability to coastal processes: The case study of Naples Gulf (southern Italy), Ocean & Coastal Management, 179, 104876, https://doi.org/10.1016/j.ocecoaman.2019.104876, 2019.

Mayer, L., Jakobsson, M., Allen, G., Dorschel, B., Falconer, R., Ferrini, V., Lamarche, G., Snaith, H., and Weatherall, P.: The Nippon Foundation—GEBCO Seabed 2030 Project: The Quest to See the World's Oceans Completely Mapped by 2030, Geosciences, 8, 63, https://doi.org/10.3390/geosciences8020063, 2018.

Milia, A.: Aggrading and prograding infill of a peri-Tyrrhenian Basin (Naples Bay, Italy), Geo-Marine Letters, 19, 237–244, https://doi.org/10.1007/s003670050114, 1999.

Milia, A.: The Dohrn canyon: a response to the eustatic fall and tectonic uplift of the outer shelf along the eastern Tyrrhenian Sea margin, Italy, Geo-Marine Letters, 20, 101–108, https://doi.org/10.1007/s003670000044, 2000.

Milia, A., Torrente, M. M., Russo, M., and Zuppetta, A.: Tectonics and crustal structure of the Campania continental margin: relationships with volcanism, Mineralogy and Petrology, 79, 33–47, https://doi.org/10.1007/s00710-003-0005-5, 2003.

Miramontes, E., Déverchère, J., Pellegrini, C., & Chiarella, D.: Mediterranean Sea evolution and present-day physiography. In Oceanography of the Mediterranean Sea (pp. 13-39). Elsevier, 2023.

Mohammadloo, T. H., Snellen, M., Renoud, W., Beaudoin, J., and Simons, D. G.: Correcting Multibeam Echosounder Bathymetric Measurements for Errors Induced by Inaccurate Water Column Sound Speeds, IEEE Access, 7, 122052–122068, https://doi.org/10.1109/ACCESS.2019.2936170, 2019.

Moussat, E., Rehault, J.-P., Fabbri, A., and Mascle, G.: Evolution géologique de la Mer Tyrrhénienne, Comptes Rendus de l'Académie des Sciences, Paris, 301, série II, 7: 491-496., 1985

Myers, N., Mittermeier, R. A., Mittermeier, C. G., da Fonseca, G. A. B., and Kent, J.: Biodiversity hotspots for conservation priorities, Nature, 403, 853–858, https://doi.org/10.1038/35002501, 2000.

Orsi, G., D'Antonio, M., Vita, S. de, and Gallo, G.: The Neapolitan Yellow Tuff, a large-magnitude trachytic phreatoplinian eruption: eruptive dynamics, magma withdrawal and caldera collapse, Journal of Volcanology and Geothermal Research, 53, 275–287, https://doi.org/10.1016/0377-0273(92)90086-S, 1992.

Passaro, S., Genovese, S., Sacchi, M., Barra, M., Rumolo, P., Tamburrino, S., Mazzola, S., Basilone, G., Placenti, F., Aronica, S., and Bonanno, A.: First hydroacoustic evidence of marine, active fluid vents in the Naples Bay continental shelf (Southern Italy), Journal of Volcanology and Geothermal Research, 285, 29–35, https://doi.org/10.1016/j.jvolgeores.2014.08.001, 2014.

Passaro, S., Tamburrino, S., Vallefuoco, M., Tassi, F., Vaselli, O., Giannini, L., Chiodini, G., Caliro, S., Sacchi, M., Luca Rizzo, A., et al. Seafloor doming driven by degassing processes unveils sprouting volcanism in coastal areas. Sci. Rep., 6, 22448, 2016.

Passaro, S., Sacchi, M., Tamburrino, S., and Ventura, G.: Fluid Vents, Flank Instability, and Seafloor Processes along the Submarine Slopes of the Somma-Vesuvius Volcano, Eastern Tyrrhenian Margin, Geosciences, 8, 60, https://doi.org/10.3390/geosciences8020060, 2018.

Pellegrini, C., Saliu, F., Bosman, A., Sammartino, I., Raguso, C., Mercorella, A., & Rovere, M.: Hotspots of microplastic accumulation at the land-sea transition and their spatial heterogeneity: The Po River prodelta (Adriatic Sea). Science of The Total Environment, 895, 164908, https://doi.org/10.1016/j.scitotenv.2023.164908, 2023.

Puig, P., Canals, M., Company, J. B., Martín, J., Amblas, D., Lastras, G., Palanques, A., and Calafat, A. M.: Ploughing the deep sea floor, Nature, 489, 286–289, https://doi.org/10.1038/nature11410, 2012.

R Core Team: R: A Language and Environment for Statistical Computing, Vienna, Austria, 2019.

Romano, P., Santo, A., Voltaggio, M. L'evoluzione geomorfologia della Pianura del fiume Volturno (Campania) durante il tardo Quaternario (Pleistocene medio-superioreOlocene). Il Quaternario 7(1): 41–56, 1984.

Ruberti, D., Buffardi, C., Sacchi, M., and Vigliotti, M.: The late Pleistocene-Holocene changing morphology of the Volturno delta and coast (northern Campania, Italy): Geological architecture and human influence, Quaternary International, 625, 14–28, https://doi.org/10.1016/j.quaint.2022.03.023, 2022.

Russo, G., Donato, R., and Di Stefano, F.: Gli habitat sottomarini delle coste della Campania, Biologi Italiani, 6, 2008.

Sacchi, M., Insinga, D., Milia, A., Molisso, F., Raspini, A., Torrente, M. M., and Conforti, A.: Stratigraphic signature of the Vesuvius 79 AD event off the Sarno prodelta system, Naples Bay, Marine Geology, 222–223, 443–469, https://doi.org/10.1016/j.margeo.2005.06.014, 2005.

Sacchi, M., Molisso, F., Violante, C., Esposito, E., Insinga, D. D., Lubritto, C., Porfido, S., and Toth, T.: Insight into flood dominated, mixed sliciclastic-volcanoclastic fan deltas: very high-resolution seismic examples off the Amalfi cliffed coast, Eastern Tyrrhenian Sea, in: Geohazard in rocky coastal areas, edited by: Violante, C., Geological Society, London, UK, 32–71, 2009.

Sacchi, M., Pepe, F., Corradino, M., Insinga, D.D., Molisso, F., Lubritto, C.: The Neapolitan Yellow Tuff caldera offshore the Campi Flegrei: Stratal architecture and kinematic reconstruction during the last 15ky, Marine Geology, 354, 15-33, 2014

Sacchi, M., Caccavale, M., Corradino, M., Esposito, G., Ferranti, L., Hámori, Z., † F., Insinga, D., Marino, C., Matano, F., Molisso, F., Natale, J., Passaro, S., Pepe, F., and Toth, T.: The use and beauty of ultra-high-resolution

691 seismic reflection imaging in Late Quaternary marine volcaniclastic settings, Napoli Bay, Italy, Földtani Közlöny,
692 149, 371, https://doi.org/10.23928/foldt.kozl.2019.149.4.371, 2019.

693 Sappington, J. M., Longshore, K. M., and Thompson, D. B.: Quantifying Landscape Ruggedness for Animal
694 Habitat Analysis: A Case Study Using Bighorn Sheep in the Mojave Desert, The Journal of Wildlife Management,
695 71, 1419–1426, https://doi.org/10.2193/2005-723, 2007.

696 Sievers, J., Milbradt, P., Ihde, R., Valerius, J., Hagen, R., and Plüß, A.: An integrated marine data collection for
697 the German Bight – Part 1: Subaqueous geomorphology and surface sedimentology (1996–2016), Earth System
698 Science Data, 13, 4053–4065, https://doi.org/10.5194/essd-13-4053-2021, 2021.

699 Slootman, A., & Cartigny, M. J.: Cyclic steps: review and aggradation-based classification. Earth-Science Reviews,
700 201, 102949, 2020.

701 Somma, R., Iuliano, S., Matano, F., Molisso, F., Passaro, S., Sacchi, M., Troise, C., De Natale, G.: High - resolution
702 morpho-bathymetry of Pozzuoli Bay, southern Italy, Journal of Maps, 12(2), 222-230, 2016.

703 Stall, S., Yarmey, L., Cutcher-Gershenfeld, J., Hanson, B., Lehnert, K., Nosek, B., Parsons, M., Robinson, E., and
704 Wyborn, L.: Make scientific data FAIR, Nature, 570, 27–29, https://doi.org/10.1038/d41586-019-01720-7, 2019.

705 Steinmann, L., Spiess, V., Sacchi, M.: The Campi Flegrei caldera (Italy): Formation and evolution in interplay with
706 sea-level variations since the Campanian Ignimbrite eruption at 39 ka. Journal of Volcanology and Geothermal
707 Research 327, 361-374, 2016.

708 Tanhua, T., Hainbucher, D., Cardin, V., Álvarez, M., Civitarese, G., McNichol, A. P., and Key, R. M.: Repeat
709 hydrography in the Mediterranean Sea, data from the *Meteor* cruise 84/3 in 2011, Earth System Science Data, 5,
710 289–294, https://doi.org/10.5194/essd-5-289-2013, 2013.

711 Taviani, M., Angeletti, L., Cardone, F., Montagna, P., and Danovaro, R.: A unique and threatened deep water coral-
712 bivalve biotope new to the Mediterranean Sea offshore the Naples megalopolis, Sci Rep, 9, 3411,
713 https://doi.org/10.1038/s41598-019-39655-8, 2019.

714 Trincardi, F., and Zitellini, N.: The rifting of the Tyrrhenian basin. Geo-Marine Letters, 7, 1-6,
715 https://doi.10.1007/BF02310459, 1987.

716 Trincardi, F., Francocci, F., Pellegrini, C., Ribera d'Alcalà, M., and Sprovieri, M.: Chapter 13 - The Mediterranean
717 Sea in the Anthropocene, in: Oceanography of the Mediterranean Sea, edited by: Schroeder, K. and Chiggiato, J.,
718 Elsevier, 501–553, https://doi.org/10.1016/B978-0-12-823692-5.00013-3, 2023.

719 Violante, C., Budillon, F., Esposito, E., Porfido, s., Vittori, E.: Submerged hummocky topographies and relations
720 with landslides, northwestern flank of Ischia Island, southern Italy, in: Proceedings of the International Workshop
721 on Occurrence and mechanisms of flow-like landslides in natural slopes and earthfills, Sorrento, Italy, May 2003,
722 14-16, 2003.

723 Walbridge, S., Slocum, N., Pobuda, M., and Wright, D.: Unified Geomorphological Analysis Workflows with
724 Benthic Terrain Modeler, Geosciences, 8, 94, https://doi.org/10.3390/geosciences8030094, 2018.

Weiss, A. D.: Topographic positions and landforms analysis, Poster Presentation, ESRI User Conference, San Diego, CA, 2001.

Worm, B., Barbier, E. B., Beaumont, N., Duffy, J. E., Folke, C., Halpern, B. S., Jackson, J. B. C., Lotze, H. K., Micheli, F., Palumbi, S. R., Sala, E., Selkoe, K. A., Stachowicz, J. J., and Watson, R.: Impacts of Biodiversity Loss on Ocean Ecosystem Services, Science, 314, 787–790, https://doi.org/10.1126/science.1132294, 2006.